

AN EXPERIMENTAL APPROACH TO STUDY ALLOMETRIC SCALING OF METABOLIC ACTIVITY

A THESIS SUBMITTED IN PARTIAL FULFILMENT OF
THE REQUIREMENTS FOR THE DEGREE OF

MASTER OF SCIENCE (RESEARCH)

BY

ADITYA ANANTHANARAYANAN IYER
UNDERGRADUATE PROGRAMME
INDIAN INSTITUTE OF SCIENCE



AFFILIATED WITH

DR. VISHWESHA GUTTAL

CENTRE FOR ECOLOGICAL SCIENCES
INDIAN INSTITUTE OF SCIENCE

SUPERVISED BY

DR. SHASHI THUTUPALLI

NATIONAL CENTER FOR BIOLOGICAL SCIENCES
TATA INSTITUTE OF FUNDAMENTAL RESEARCH

JUNE 2020

Certificate

Mr Aditya Ananthanarayanan Iyer has worked under my supervision between August 2019 and June 2020. I have gone through his work on '*An experimental approach to study allometric scaling of metabolic activity*' presented in this thesis, and have found it to be satisfactory.

Dr. Vishwesha Guttal
Center for Ecological Sciences
Indian Institute of Science

Dr. Shashi Thutupalli
National Center for Biological Sciences

I, Aditya Ananthanarayanan Iyer, have worked on a project to establish *An experimental approach to study allometric scaling of metabolic activity*, under the supervision of Dr. Shashi Thutupalli (NCBS) and Dr. Vishwesha Guttal (CES, IISc), between August 2019 and June 2020. No unfair means have been used at any point during this project.

Aditya Ananthanarayanan Iyer
Undergraduate Program (Biology)
Indian Institute of Science, Bengaluru

Contents

1 Allometric Scaling of Metabolic Rate	1
1.1 Models Explaining the Scaling Exponent	3
1.1.1 Physical models	4
1.1.2 Cellular Models	5
1.1.3 Organismal models	6
1.1.3.1 Wittig Model for Foraging	6
1.1.3.2 Allometry as a By Product of Body Size Optimization	6
1.1.4 Resource Transport Models	6
1.1.4.1 Supply Demand Balance - The Banavar - Maritan - Rinaldo Model . .	8
1.1.4.2 The Unified Theory for Metabolic Scaling	8
1.1.5 The Dynamic Energy Budget model	9
1.1.6 Other Recent Theories	10
1.1.6.1 Quantum Metabolism Theory	10
1.1.6.2 Self Organised Criticality - 3/4 is an evolutionary accident	11
1.1.6.3 Thermodynamic Origin Model	11
1.1.6.4 Allometric Cascade Model	11
1.1.6.5 Metabolic Level Boundary Hypothesis	12
1.2 Shifts in Perspective on Metabolic Scaling	12
1.3 Why is it so complex?	13
1.4 Experimental Studies on Metabolic Scaling	14
References	14
2 The Snowflake Yeast	19
2.1 Appeal as a Model System for Metabolic Scaling	20
2.2 Characterization of the Model System	20
2.3 Measuring Mass of the Snowflakes	24
2.3.1 Filter Technique	24
2.3.2 Volume and Density	25
2.3.2.1 Density Measurement	25
2.3.2.2 Volume Measurement	27
2.4 Concluding Statements	28
References	28

3 Measuring Metabolic Activity	30
3.1 Single Cell Metabolic Activity - A Microfluidic Method	31
3.2 A Droplet-in-Droplet Method	32
3.3 Caveats	44
References	45
4 Discussion	48
4.1 The Yeast Snowflake - An experimental model for allometry	48
4.2 The Droplet-in-Droplet method for measuring metabolic activity	49
4.3 Implications from Allometric Scaling of Metabolic Activity	50
References	50
Appendix: The Droplet in Droplet Method	52
References	55
Acknowledgements	56

List of Figures

1.1 Kleiber (1932) proposed that the allometric scaling exponent for metabolic activity, measured as heat produced is close to 0.75. Backed by empirical evidence, this challenged the prevailing notion of the time, that the exponent was 2/3, from surface area relationships (See text)	2
1.2 The scaling relationship between metabolic activity and mass seems to hold true for a large range of masses, across different taxonomic group. Plot obtained from Thommen et al. 2019, with data from Makaireva et al. 2008.	4
2.1 Images of different populations of the snowflake yeast. The selection protocol for these populations are given in Table1. Note that G7 has more elongated cells than the other populations	21
2.2 Time series of size distributions of a snowflake after chitinase action. The protocol is described in the text. Note that the variation is least at 14 hours.	22
2.3 Size of the yeast snowflake of different populations at the timepoint where the size distributions were the tightest. Note that G6, G7, G8 have not been analysed. With these populations, the size variation across the plot would be higher. Also, the area of the top view of the snowflake is being plotted on the Y Axis	23
2.4 Characterising the filter method for mass measurement. Different dilutions of the same culture of yeast cells were used to estimate mass. The mass difference $M_2 - M_1$ (see text) is plotted against the dilution factor.	25
2.5 Densities of the snowflake populations estimated from Percoll based Density Gradient Centrifugation. Coloured density bead markers are used for calibrations. The densities vary across populations.	26
2.6 Schematic for measuring volume from depth sectioned images	27
3.1 A grid of aqueous droplets with YPD and cells. Over time, as cells start to consume metabolites, the metabolite concentrations fall. In response to the change in concentration gradient, water flows out of the droplet with the cell. The inset shows an example of such a droplet	31
3.2 Schematic of droplet set-up used. An aqueous droplet with a concentration of solutes (S_1) is trapped in a droplet of fluorinated oil. The droplet in droplet system is placed in an aqueous bath, with solute concentration S_2 . If $S_1 < S_2$, water can flow out of the droplet in response to the osmotic gradient	33

3.3	Image of droplet-in-droplet setup. In the ideal scenario, all the packed oil droplets would have a single aqueous droplet. The aqueous droplets are in contact with the outer aqueous bath	33
3.4	With no concentration gradient, the droplet sizes do not change with time. The setup had 20g/L glucose solution in the aqueous droplet and the bath.	35
3.5	With 1M EtOH in the aqueous droplet, there is no shrinkage. The setup had 1M EtOH in 20g/L glucose solution in the aqueous droplet and 20g/L glucose solution in the bath. 107 droplets were analysed for this control	36
3.6	The droplet radius shrinkage is linear with time when there are no solute molecules in the aqueous droplet. In this setup, the inner droplet has water, and the outer bath is a 20g/L glucose solution. 29 droplets were analysed.	37
3.7	The droplet radius shrinkage is linear with time when there are no solute molecules in the aqueous droplet. In this setup, the inner droplet has water, and the outer bath has YPD	38
3.8	With YPD diluted to twice its volume in the droplet, and YPD in the bath, the droplet shrinkage is as given. The droplet stops shrinking when the concentrations inside the droplet matches with the bath. The inset histogram shows the distribution of fits for the constant in Equation 3. 87 droplets were analysed.	39
3.9	Some examples of fits of Equation 3 (blue) to droplet shrinkage dynamics (red) for droplets with YPD diluted to four times, in a bath of YPD. R^2 is estimated using the first 20 points of the dataset	40
3.10	With YPD diluted to four times its volume in the droplet, and YPD in the bath, the droplet shrinkage is as given. The droplet stops shrinking when the concentrations inside the droplet matches with the bath. The inset histogram shows the distribution of fits for the constant in Equation 3.	41
3.11	Some examples of fits of Equation 3 (blue) to droplet shrinkage dynamics (red) for droplets with YPD diluted to four times, in a bath of YPD. R^2 is estimated using the first 20 points of the dataset	42
3.12	The Droplet in Droplet system with cells. Ideally, each oil droplet has one aqueous droplet, and each aqueous droplet starts with a single cell. Over time the cell consumes glucose, and the droplet shrinks	43
3.13	Droplet Shrinkage for the droplets containing cells (Gray and Blue plots correspond to one droplet each). They seem to follow the same trajectories.	44
4.1	A flow focusing device is used for generating mono-disperse aqueous droplets. Image by Akshaya Iyer	53
4.2	T junction device for generating the droplet in droplet setup. Image by Akshaya Iyer . .	54
4.3	Schematic outline for preparing a mold for a device and the PDMS device that can be used for micro-fluidics. Image by Yash Rana	55

Abstract

The power law relationship between metabolic activity and body size, prevalent across most taxonomic groups, is a puzzling correlation. Over the last century, many theories have been proposed to explain this apparent scaling law. There are countless records of empirical data supporting the allometric scaling of metabolic rates. The lack of consensus on the physical basis of the scaling relationship can be attributed to the absence of suitable model systems with large variation in body size, and experimental manipulability.

The snowflake yeast, an experimentally evolved *Saccharomyces cerevisiae* based model, which exhibits over 6 orders of magnitude of variation in body size is proposed as a potential experimental system for exploring the relationship between metabolic activity and organism size.

Additionally, a microfluidic technique for measuring metabolic activity from single cells and individual aggregates of cells, like the yeast snowflake is described.

Chapter 1

Allometric Scaling of Metabolic Rate

In an influential review from 1966, Gould describes allometry as the study of size and its consequences (*Gould 1966*). Historically, allometry was driven by observations that the proportion of parts of an organism change consistently as the total size changes. Following correlative studies, such as those of brain size vs body size in mammals (*Dubois 1897*) and of the relative size of secondary sexual characters in beetles as a function of body size (*Champy 1924*), it was observed that the correlations seemed to follow a power law relationship:

$$y = bM^\alpha$$

where y is the parameter under consideration, M is the mass of the organism, and b and α are physiological constants. The value of the scaling exponent α has been a point of contention within the expansive field of allometry (*D. Glazier 2018; Makarieva et al. 2008; Kearney & White 2012; White & Kearney 2014*). It indicates possible constraints on the organism, universal to life, and with deep, important implications in physiology and evolution (*D. Glazier 2014; Kleiber 1947*). von Bertalanaffy showed that if two physiological parameters grow by first order kinetics, the parameters should be correlated by a power law relationship (*Bertalanaffy 1949*).

Such allometric relations for different physical and physiological parameters were observed and characterised across four paradigms; ontogeny (across development), phylogeny (across lineages), intraspecifically and interspecifically. A grouping like this allowed for structured thought on the possible physical bases of observed allometries (*Gould 1966*).

Metabolic activity, being an indicator of the ‘pace of life’ was also subject to such correlative allometric studies (*Kleiber 1947; Kleiber et al. 1932*). It was noted quite early (read 1839) that metabolic activity might not scale linearly with size, citing the physical constraints that volume poses on surface areas (*Sarrus 2017*). With an initial empirical data gathering study using different breeds of dogs, Max Rubner proposed that metabolic rate should follow the allometric scaling relation with an exponent of $2/3$, formalising the surface area hypothesis. The constraints posed by surface area on uptake and heat loss formed the basis of this hypothesis (*Rubner 1883*).

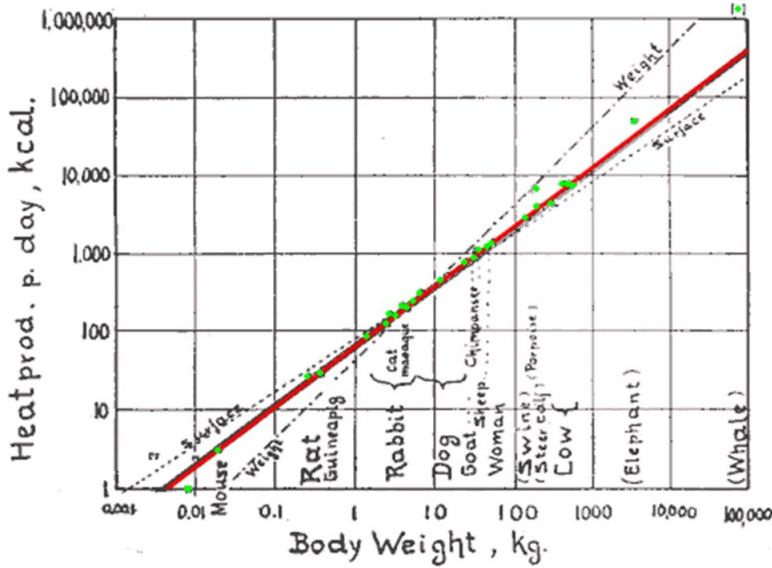


Fig. 1. Log. metabol. rate/log body weight

Figure 1.1: Kleiber (1932) proposed that the allometric scaling exponent for metabolic activity, measured as heat produced is close to 0.75. Backed by empirical evidence, this challenged the prevailing notion of the time, that the exponent was 2/3, from surface area relationships (See text)

The use of dimensional analysis & similarity criteria by D'arcy Thompson in his discussions on allometric and isometric scaling effects to locomotion (*Thompson 1942*) inspired a branch of researchers to develop similar models for metabolic scaling. Metabolic rate is, in dimensional terms, energy per unit time. As a power function of mass, length and time, the metabolic rate (Q) can be represented as $Q = ML^2T^{-3}$. Assuming geometric similarity, constancy of density and linear scaling of time with length, Lambert and Tessier proposed a formal natural explanation for the 2/3 scaling exponent using dimensional analysis (*Lambert & Tessier 1927*).

But, a larger empirical collection of data on metabolic rates and size (*Kleiber et al. 1932*) seemed to indicate that the exponent was closer to 0.75, thereby challenging the physical bases of then existing models. The indication was further supported by a multitude of empirical data collection studies that followed Kleiber (*Kleiber 1947; Kleiber et al. 1961*). Metabolic activity from unicellular organisms to blue whales, i.e over 21 orders of magnitude in mass, seemed to conform to a scaling exponent of close to 0.75 (*Brody 1945; Makarieva et al. 2008*).

There was also a parallel school of thought that claimed that the scaling exponent of 0.75 was a statistical artifact (*Heusner 1982*). Different analyses of separate classes of organisms revealed differing exponents (*Dodds et al. 2001*). In birds, the exponent for passerines were found to be 0.72. But, if passerines and non-passerine were analyzed together, the exponent was estimated at 0.67 (*Lasiewski & Dawson 1967*). Analysis of metabolic rates from unicellular organisms revealed an exponent of 0.60 (*Prothero 1986*). Inclusion and exclusion of data leads to different exponent fits, casting doubts on the 'universality' of an exponent in the relationship between metabolic activity and mass (*Dodds et al. 2001; Agutter & Wheatley 2004*). There are arguments about which regression methods of fitting data to use for metabolic rate and mass. The commonly used approach is the Ordinary Least Squares

(OLS) Method. But, the underlying assumptions are that the mass has to be measured without error, and that the data being compared are independent (*White & Kearney 2014*). The other suggested approach is the Reduced Major Axis (RMA) Method, which is free from the limitations of the OLS, with the caveat that variances in mass and metabolic rate are assumed equal (*White & Kearney 2014*). The choice of the method of regression becomes more important in a log-log plot, as the log-log transformation could introduce bias (*White & Kearney 2014*). Some even doubt that the power law is the best fit, instead suggesting correction terms, like $MR = M^b + c$, or $MR = M^b 10^\epsilon$ (*Hui & R. B. Jackson 2007; Kearney & White 2012*). In 2010, Kolokotrones et al. proposed a new perspective on the matter of metabolic scaling, suggesting a 5 parameter model to explain the curvilinear trend of the convex curvature in metabolic rates at higher masses (*Kolokotrones et al. 2010*).

There is debate on interpreting metabolic activity too. There are 4 major kinds of metabolic activity; tissue-maintainence (TMR), basal (BMR), maximal (MMR), and field metabolic rate (FMR) (*J. K. L. da Silva et al. 2006*). The TMR is the lowest metabolic rate for supporting life (generally in torpid/hibernating animals). BMR is the metabolic rate required to support tissues and essential life functions in non-torpid animals. MMR is the metabolic rate when the organism is being exerted to its maximum capacity. FMR is the metabolic activity averaged over the day. The allometric scaling of these metabolic activities are not similar (*J. K. L. da Silva et al. 2006; D. Glazier 2018*). The constraints posed for these different kinds of metabolic activity would differ. Additionally, is it intuitive to compare metabolic activity across species, given the variation in the factors involved? Metabolic rates were measured using food uptake, heart rates, calorimetry outputs, and respirometry readouts (*Kearney & White 2012*). Could a simple arithmetic operation for converting between such measurements allow for comparisons?

Nonetheless, some studies have, with appropriate correction coefficients for temperature, phylogenetic grouping and method of measurement, attempted to quantify the exponent in parts. In 1988 McNab collected and analysed published data on basal metabolic activity and mass from 321 species. While ruling out the existence of a universal scaling, he states that for masses less than 300g, an exponent of 0.6 best fits the data. At larger masses, the 0.75 exponent is supported (*McNab 1988*). In 2010, Isaac et al. compiled data from 1242 species, and stated that exponents varying across taxonomic groups better described the data than a single universal exponent (*Isaac & Carbone 2010*). However, the mean exponent from the different taxonomic groups was very close to 0.75. Makarieva et al. 2010 compiled a larger dataset, comprising of 3006 species, and rejected the null hypothesis of both 0.67 and 0.75 as a universal scaling exponent. The compiled data indicates that ‘mean mass-specific metabolic rates converge on a relatively narrow range’, suggesting some fundamental constraint linking metabolic activity and mass (*Makarieva et al. 2008*).

1.1 Models Explaining the Scaling Exponent

Following Kleiber’s study, many models and hypotheses were proposed for explaining the apparent 3/4 scaling exponent. Additional parameters and correction factors to the dimensional analysis model were considered (*Gunther 1975*). But, dimensional analyses models had only explanatory value, and almost no predictive value. The assumptions of scaling of time had no physiological or physical

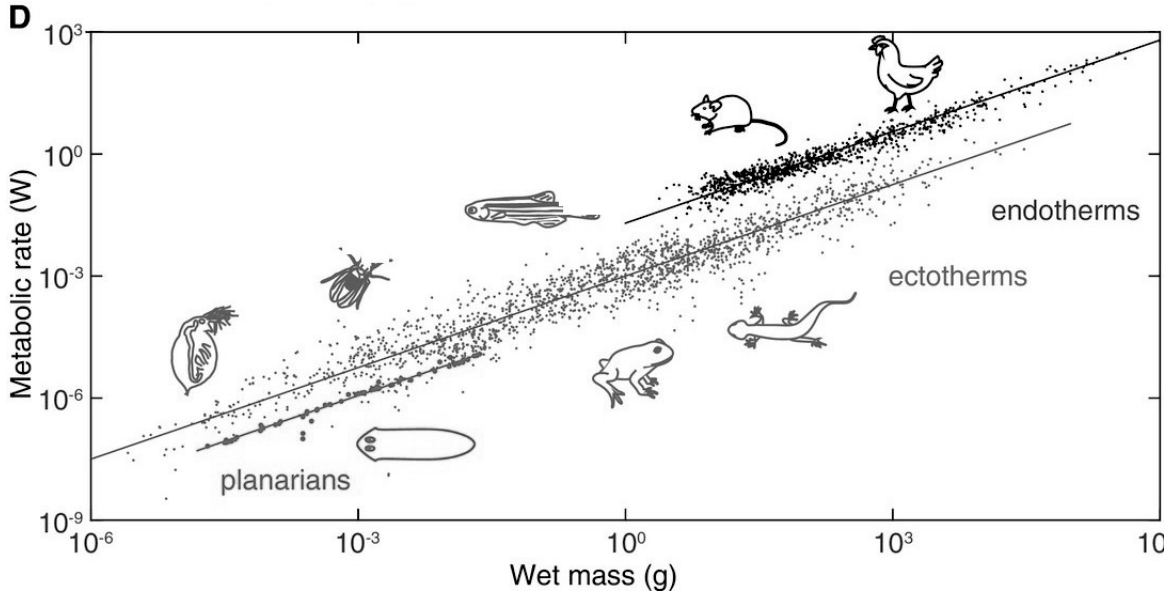


Figure 1.2: The scaling relationship between metabolic activity and mass seems to hold true for a large range of masses, across different taxonomic group. Plot obtained from Thommen et al. 2019, with data from Makaireva et al. 2008.

basis. In addition, the logic and applicability of such models to biological parameters were also found questionable (*Butler et al. 1987*). The following sub-sections describe some of the numerous models that have been proposed. For a thorough review of this discussion, see (*D. Glazier 2014; J. K. L. da Silva et al. 2006; Agutter & Tuszynski 2011*).

1.1.1 Physical models

One of the first successful models in this endeavor explained the $3/4$ scaling as a consequence of physical constraints on body proportions and work done by muscles (*McMahon 1973*). McMahon derived the maximum possible length of a cylindrical muscle, without it buckling or bending due to physical forces. The critical length (l) was found to be proportional to $(E/\rho)^{1/3}d^{2/3}$ where E is the elastic modulus, ρ is the density and d the diameter. Assuming that all proportions of an organism scale the same way, the mass can be written as $M \propto ld^2$. Using the previously derived length constraint, the diameter is then proportional to $M^{3/8}$. Now, for a muscle of cross sectional area A , shortening by a length Δl in time Δt with a strain of σ , the power exerted by the muscle is $\sigma A \Delta t / \Delta L$. Empirical evidence at the time suggested that σ and $\Delta t / \Delta L$ were constant in a muscle across species (*Hill 1950*). Therefore, the power exerted by the muscle, synonymous with its metabolic rate is proportional to the cross sectional area, i.e. metabolic rate MR scales with d^2 . Using the relationship between d and mass, $MR \propto (M)^{3/4}$.

Although the McMahon model provides a physical basis for the $3/4$ scaling law, there are primarily three lines of arguments against it. (1) Sea mammals are not subject to the physical constraints posed by gravity on buckling and bending. Yet, they exhibit $3/4$ scaling. The model also fails for unicellular organisms for which gravity is not the constraining external force. (2) The assumption of $\Delta t / \Delta L$ being constant implies that time scales with length, which was a point of contention with dimensional

analysis models too. (3) More importantly, muscle contraction makes up a very small fraction of total metabolic activity of an organism (*Seeherman et al. 1981*).

Another model which received some attention in the 1980s attempted to explain metabolic rate scaling with mass as a mixed effect of surface area (which scales as $2/3$ with volume) and response to gravity (which scales linearly with mass) (*Economos 1979*). Economos fit extant empirical data on metabolic scaling using an empirical relation; $MR = A.M^{2/3} + B.M^{0.89}$ where A and B are constants relating to surface area effects and gravity effects respectively. Relying on gravity, the model fails to explain metabolic rate scaling in organisms for which other physical forces are more dominant. In addition, the data fitting model lacks a physiological explanation of the mixed effects of surface area scaling and response to gravity (*Agutter & Wheatley 2004*).

In the early 1980s, Coulson and his collaborators characterised the constraints posed on blood flow with body size and the implications to metabolic activity. Noting that the interaction with enzymes depends on the flow rate of resources, metabolic activity was estimated as a function of flow rate, which, in turn is assumed to be dependent on body size (*Coulson 1986*). A more physical argument for resource flow constraining metabolic activity was given by Patterson (*Patterson 1992*). In algae and invertebrate aqueous organisms, the metabolic uptake is driven by diffusion across a boundary layer. Considering the constraints posed by fluid convection on mass transfer across the boundary layer, the metabolic rate exponent for calculated for simple organism geometries; flat plate, sphere and cylinders. This model, derived from first principles had good agreement with empirical data in sea anemones and algae. Unfortunately, it could not be generalised. Most organisms actively ingest and do not rely only on diffusion for intake. In addition, the drawbacks of assuming supply limited metabolic activity, as opposed to demand limited still prevailed (*J. K. L. da Silva et al. 2006; Agutter & Tuszynski 2011*).

In a short article from 1977, Blum noted that if organisms had 4 dimensions instead of 3, the $3/4$ scaling exponent follows naturally. For an organism in 4 dimensional space, surface area scales as $3/4$ with volume (*Blum 1977*). Time has been proposed as a possible fourth dimension in some models (*J. K. da Silva et al. 2007; Ginzburg & Damuth 2008; D. West & B. J. West 2013*). The highly popular model proposed by West, Brown and Enquist (1997) claimed that the fractal, space filling nature of resource distribution networks can be characterised as four dimensional (*G. B. West et al. 1997; G. B. West et al. 1999*). This model will be discussed in a later section.

1.1.2 Cellular Models

In a series of historical papers, von Bertalanffy (*Bertalanffy 1949; Von Bertalanffy 1957*) identified three different metabolic types according to the dependence of metabolic rate on body size. The first, scaling sub linearly, as defined by surface area, with an exponent of $2/3$. The second, scaling linearly, i.e. proportional to the volume of the organism. For the third type, the scaling exponent is expected to be between $2/3$ and 1. This classification was given a physiological basis in a discussion by Davison. He proposed that if increase in mass is achieved through increase in cell number, the metabolic rate scales linearly with mass (*Davison 1955*). But, if the increase in body mass is caused by an enlargement of cells, by surface area arguments, metabolic rate should scale with an exponent

of 2/3. The observed scaling of metabolic rates could be due to a mixed interaction of the two modes for increasing body mass. The hypothesis does not explicitly state why the mixed interactions would correlate to an exponent close to 3/4 consistently across life.

Some reports suggested the existence of a strong correlation between the genome size and cell size in eukaryotes (*Gregory 2001; Szarski 1970*). Deriving from von Bertalanffy, the body size correlates with the genome size and cell number. Kozłowski et. al., in 2003 proposed that metabolic activity also varies with the genome size. Smaller cells enable rapid conversion of energy to tissues, whereas large cells enable long fasting periods (*Kozłowski et al. 2003*). Therefore, body size and metabolic activity are not independent variables, but are related through genome size. Kozłowski et al. proposed this as a potential evolutionary mechanism for the existence of the metabolic scaling exponent. The model explains the allometric exponent in many orders of birds and mammals. However, a more recent meta-analysis confirmed that there is no correlation between genome size and basal metabolic activity in vertebrates (*Gardner et al. 2020*).

1.1.3 Organismal models

1.1.3.1 Wittig Model for Foraging

Where other models attempted to explain the scaling exponent from cellular and physiological processes, the Wittig model attempted to explain the exponent using the organismal-level process of foraging. The model attempted to quantify constraints posed on foraging, and by extension on food intake of an organism. Assuming that foraging efficiency and food intake is constrained by self inhibition (as foraging increases, food availability reduces), and competition with conspecifics (more competition, less availability), Wittig derived the metabolic scaling exponent to be 0.75 for organisms foraging in two dimensions. The model also correctly predicts the exponent being closer to 0.83 for organisms foraging in 3 dimensions, such as lizards, turtles and fishes (*Witting 1998*).

1.1.3.2 Allometry as a By Product of Body Size Optimization

This model assumes optimal allocation of resources to growth and reproduction as a result of natural selection. Consequently, this optimal allocation translates to optimisation of body size. Kozłowski and Weiner claim that the allometric exponents are statistical results of this optimisation, when considered with intra-species distributions of production and mortality rates. But, it can also be argued that the model simply shifts the burden of explaining metabolic scaling exponents to explaining the distributions of production and mortality rates (*Kozłowski & Weiner 1997*)

1.1.4 Resource Transport Models

In 1997, West, Brown and Enquist (WBE) proposed a model explaining the 3/4 metabolic scaling exponent by imposing constraints on resource distribution networks in organisms. They based the model on three main assumptions. Firstly, the resource distribution network should cover the entire volume of the organism. This is achieved by a space filling, fractal like branching pattern. Secondly, the

final branch in the networks, i.e. the terminal units are size invariant. Finally, the resource distribution network is optimised for energy efficiency (through natural selection) (*G. B. West et al. 1997*)

Assuming that the network is composed of N branchings, and each branch branches into n_k branches, the total number of vessels at any level k is given by $N_k = n_0 n_1 n_2 \dots n_{k-1}$. Here, n_0 is the number of branches from the primary vessel. At each branch, the radius and length of the vessel reduces. Hence, two ratios γ_k and β_k can be defined at each branch to capture the change in length and radius, respectively. $\gamma_k = l_{k+1}/l_k$ and $\beta_k = r_{k+1}/r_k$ (*G. B. West et al. 1997*)

To impose the energy minimization assumption, the resistance to flow in the entire network should be minimised. Assuming pressure induced Poisuelle flow through a rigid pipe, the impedance of the network Z is calculated. Minimizing this impedance while enforcing the constraint of space filling leads to the following features that the network should comply to. Firstly, the number of branchings at each level is the same, $n_i = n$. Secondly, the volume supplied by each level should be the same. Thirdly, the sum of cross-sectional areas of the daughter branches should equal the cross sectional area of the parent branch. Finally, the volume of flow is proportional to the mass of the organism. $V \propto M$.

Using these relationships, we have $N_k l_k^3 = N_{k+1} l_{k+1}^3$ and $\pi r_k^2 = n \pi r_{k+1}^2$. Given $N_{k+1}/N_k = n$, this leads to $l_{k+1}/l_k = \gamma_k = n^{-1/3}$ and $r_{k+1}/r_k = \beta_k = n^{-1/2}$. All the γ_k and β_k are equivalent.

If the velocity of flow at level k is denoted by u_k , the volume flow rate through the vessel is $\dot{Q}_k = \pi r_k^2 u_k$. By conservation of fluid flow, the volume flow rate through the primary vessel should be the sum of the flow rates at each of the terminal capillaries (level c). $\dot{Q}_0 = N_c \dot{Q}_c = N_c \pi r_c^2 u_c$. \dot{Q}_0 represents the rate of flow of oxygen and nutrients too. Therefore, the metabolic rate is expected to be proportional to \dot{Q}_0 . Invoking the second assumption of size invariance of terminal units, $B \propto \dot{Q}_0 = N_c \pi r_c^2 u_c \propto N_c$, i.e. $B \propto n^n$.

The volume of flow, which is proportional to mass can be represented as $V = \sum_{k=0}^N N_k V_k = \sum_{k=0}^N n^k \pi r_k^2 l_k$. Using the relationships of γ and β , this can further be reduced in terms of the size invariant terminal units (Assumption 3). At the limits where the number of branchings is large, $V \propto (\gamma \beta^2)^{-n}$, i.e. $V \propto n^{4n/3}$.

The authors derived that the mass M , proportional to the volume scales as $n^{4n/3}$ with n branchings at each level, and that metabolic activity B , proportional to flow rate n^n . Comparing these relationships, $B \propto M^{3/4}$, the mysterious scaling exponent of $3/4$ is obtained.

This was an elegant derivation for the $3/4$ scaling exponent. The WBE model reignited the quest for explaining the exponent, and led to a boom in this field. The model has been heavily critiqued since its proposal, for its assumptions, derivation and conclusions (*D. Glazier 2014; Dodds et al. 2001; Kozlowski & Konarzewski 2005*). Empirical evidence goes against the size invariance of terminal units (*Kozlowski & Konarzewski 2005*). Studies across mammals suggest that $r_c \propto M^{1/12}$, and $l_c \propto M^{5/24}$. The model fails to explain scaling in insects and other organisms which don't have a cardiovascular system. Dodds et al, (2001) in a scathing review of the models proposed for metabolic scaling pointed out that the impedance calculated in the WBE model failed to account for the relationship between the velocity of pulsatile flow and the radius of the capillary. In this corrected framework, the scaling exponent was theorized to be $6/7$. In addition, the energy minimization arguments, if correctly

interpreted, do not suggest a self similar fractal network with constant n , γ and β , which is essential to the WBE model (*Dodds et al. 2001*).

Although the WBE model was flawed, it kindled the debate about the metabolic scaling, its cause, and its effects. It inspired many experimental and empirical data collection studies, and theoretical models to explain the scaling of metabolic activity with mass (*D. S. Glazier 2005; GLAZIER 2006; Savage, a. J. F. Gillooly, et al. 2004; Savage, Deeds, et al. 2008; Agutter & Wheatley 2004*).

In 1999, West, Brown and Enquist suggested another explanation for the 3/4 scaling exponent, suggesting it as a consequence of the fourth dimension of life (Blum), which appears because of the fractal nature of the resource distribution network. The surface area S and volume V are related by $S^{1/(2+\epsilon_s)} \propto V^{1/(3+\epsilon_v)}$, where ϵ_s and ϵ_v are corrections to the Euclidean dimensions. (Fractal structures have non integer 'dimensions'). Assuming metabolic rate to be proportional to exchanges from the surface area (arguments from Rubner), and that density of organisms are constant, $B \propto S \propto V^{(2+\epsilon_s)/(3+\epsilon_v)} \propto M^{(2+\epsilon_s)/(3+\epsilon_v)}$. With the constraint of maximising surface area, West et al. showed that both ϵ_s and ϵ_v should be 1. With this constraint, $B \propto M^{3/4}$ (*G. B. West et al. 1999*). This model was again critiqued by Dodds et al, for the minimization procedures used, suggesting that the correctly derived exponent from the proposed model would be 1 (*Dodds et al. 2001*).

1.1.4.1 Supply Demand Balance - The Banavar - Maritan - Rinaldo Model

Banavar et al (2002) proposed another network distribution model following the WBE model. Considering a d dimensional space with $N = L^d$ distributed sites across the volume, a network is constructed such that there is atleast one path from a source node to all N sites in the d dimensional space. The source supplies nutrients, and each node consumes a bit and transfers the rest to linked sites. If the consumption at each node E is constant, the metabolic rate B is $B = L^d E$. In such a system, the mass is assumed to scale with the volume, i.e. $M \propto L^d$. Optimizing the supply network, the constraints, the total flow rate F is shown to be proportional to L^{d+1} . The extra L comes from the implied constraint of the shortest mean distance from the source to all the nodes in the optimised network. The demand of the network is characterized by the sum of demands of each node. The Banavar model claims that the scaling exponent is $d + 1/d$ for a system where supply and demand are matched. In a 3 dimensional system, the exponent of 3/4 is obtained. The authors claim that deviations observed are a result of supply demand imbalances, rising from inefficiency in the network (*Banavar, Damuth, et al. 2002; Banavar, Moses, et al. 2010*).

1.1.4.2 The Unified Theory for Metabolic Scaling

In 2006, da Silva, Barbosa and Silva proposed a theory incorporating multiple biological aspects associated with metabolism to explain the scaling exponents for different metabolic states (*J. K. L. da Silva et al. 2006; J. K. da Silva et al. 2007*). The model considers three regimes of resource transport; Diffusive, Inertial and a combination of both. The metabolic states of a d dimensional organism can be represented as a point in $(d + 1)$ dimensional space, characterised by d biological lengths (L_1, L_2, \dots, L_d) and one physiological time τ . The metabolic states can be represented by 2 size invariant quantities, mass density $\rho_{d+1}(L_1, L_2, \dots, L_d, \tau)$ and energy density $\sigma_{d+1}(L_1, L_2, \dots, L_d, \tau)$. The

mass of the system is therefore $M = \rho_{d+1}\tau V_d$, where V_d is the d dimensional volume. Similarly, total energy is $E = \sigma_{d+1}V_d\tau$. Metabolic rate, or power is energy per unit time. Using physiological time, the metabolic rate $B = \sigma_{d+1}V_d$. Comparing this relationship to that of mass, $B = (M\sigma_{d+1})/(\tau\rho_{d+1})$. Using the size invariance assumptions of the energy density and mass density, we have $B \propto M/\tau$

In organisms where diffusion is the primary mechanism of resource transport, i.e. unicellular organisms and very small organisms, the length scales and time scales can be related by the diffusion transport relationship, $L = D_0\tau^{1/2}$, where D_0 is the size invariant diffusion coefficient. With $L_1 \propto L_2 \propto \dots \propto L_d \propto L$, the mass is $M \propto \tau V_d \propto L^2 L^d$. Therefore, $L \propto M^{1/(d+2)}$. Using the diffusion transport relationship, $\tau \propto M^{2/(d+2)}$. From $B \propto M/\tau$, the allometric scaling relationship for small organisms is $B \propto M^{d/(d+2)}$. For 3D organisms, the scaling exponent is predicted to be 0.6. This prediction has empirical support from analysis of a dataset of eukaryotic unicellular organisms from 1986, which estimated the exponent to be 0.608 ± 0.05 (*Prothero 1986*).

For organisms where inertial transport is the major mechanism of resource transport (mammals for instance), $L = v_0\tau$, where v_0 is a size invariant velocity. Here $M \propto \tau V_d \propto LL^d$, i.e. $L \propto \tau \propto M^{1/(d+1)}$. From $B \propto M/\tau$, the allometric scaling relationship for organisms in this regime is $B \propto M^{d/(d+1)}$. For 3D organisms, the scaling exponent is predicted to be 3/4. Note that the derivation here is independent of the nutrient transport network structure.

The third regime is where both diffusive and inertial processes contribute to resource transport. The two time scales involved are assumed to be the same. The two length scales are assumed to be proportional. For the inertial process, $L_1 \propto L = v_0\tau$ for 1 dimension. For the diffusive processes, $L_i \propto L \propto D_0\tau^{1/2}$ for d-1 dimensions. The mass M in this regime is $M \propto \tau V_d \propto \tau v_0 D_0^{d-1} \tau \tau^{(d-1)/2}$, i.e. $M \propto \tau^{(d+3)/2}$. Inverting this relationship, $\tau \propto M^{2/(d+3)}$. From $B \propto M/\tau$, the allometric scaling relationship for organisms in this regime is $B \propto M^{(d+1)/(d+3)}$. In three dimensions, the scaling exponent is 2/3. Note that this exponent was derived without invoking surface area - volume relationships.

This unified theory for metabolic scaling explained different metabolic scaling exponents using constraints posed on resource transport by its diffusive or inertial mechanisms. The theory has empirical support too. The theory also indicates that there is no single universal allometric exponent for metabolic rates (*J. K. L. da Silva et al. 2006*).

1.1.5 The Dynamic Energy Budget model

Resource transport was not the only approach used to explain the allometric scaling exponent. A parallel approach used constraints posed by system composition and resource demand to build a framework to relate metabolic rates to body mass. The Dynamic Energy Budget (DEB) Theory (*B. Kooijman & S. Kooijman 2010*). emphasizes on the significance of physicochemical constraints on the build-up and use of stored metabolites. DEB is motivated by the observation that metabolism depends on nutritional history more than currently available feeding conditions.

Nutrient storage is an important requirement in almost all living organisms. There are strict limits on the concentration of any substrate circulating in the body, posed by limits on osmotic pressures.

Without the possibility of storage, organisms won't be able to cope with variable feeding conditions. A large fraction of ingested nutrient are therefore stored as macromolecules (*van der Meer 2006*). The non-homogeneity in storage of these macromolecules in the body implies that the periphery of these storage sites are more relevant for reaction rates than the concentrations alone. The DEB theory partitions biomass into two categories: reserve and structure (*B. Kooijman & S. Kooijman 2010*). The reserve is the pool of stored macromolecules which can be mobilized for the maintenance of structure and related processes. The surface area of the pool determines how fast the reserve can be mobilised (*B. Kooijman & S. Kooijman 2010*). Assuming that the stoichiometric relationship between the size of the reserve pool and the total structure is constant, and that a fixed proportion of energy obtained from the reserve is spent in maintenance and growth, the standard DEB model predicts the scaling exponent to be between 2/3 and 1.

The standard DEB model, in its original form is a very complicated mesh of relationships, involving innumerable factors, depending on contexts and organismal states. The DEB was not proposed only for explaining the metabolic scaling exponent. It is supposed to be a single quantitative framework for describing aspects of metabolism at the individual level, across all organisms; a formal theory of metabolism (*Maino et al. 2014*)

1.1.6 Other Recent Theories

1.1.6.1 Quantum Metabolism Theory

The relationship between metabolic rate and mass depends on metabolic activity at the cellular level. Quantum Metabolism (QM) claims that the metabolic scaling results from sub-cellular processes, and not just the geometry of the resource supply network. The underlying idea has been discussed on many occasions (*Kozłowski et al. 2003; Krebs 1950; Altman & Dittmer 1968; Rolf & G. Brown 1997; Hochachka & Somero 2002*).

The QM model assumes that energy transduction in cells is a result of coupling of 2 molecular mechanisms; the electron transport chain and the ATPase motor. Additionally, the enzymes responsible for these processes are assumed to occupy fixed localised positions in the mitochondrial membrane. In this framework, the behavior of these enzymes can be modeled as a coupled oscillator. A continuous supply of energy is expected to result in elastic vibration of the 'oscillators' (enzyme activity). Using a formulation akin to the Einstein–Debye model, the relationship between metabolic rate B and mass M is found to be $B \propto M^{d/(d+1)}$, where d is a dimensionality parameter.

The QM model explains the metabolic rate differences between cancerous cells and normal cells, dependence of metabolic rate on temperature, and large intra-taxa variations in the metabolic rate. The authors claim that the model is applicable to unicellular organisms, plants, animals and anaerobes too (*Agutter & Tuszynski 2011*).

1.1.6.2 Self Organised Criticality - 3/4 is an evolutionary accident

In dynamical systems, power laws signify criticality; criticalities are defined by the divergence of the integral of a power function (*Goldenfeld 1992*). Experimental studies in modular organisms (*Nakaya et al. 2005*) have been interpreted to indicate that self-organisation maintains the spontaneous criticality in the allometric relationship. It is often hypothesized that self organisation mediated criticality is crucial for evolution of life (*Nakaya et al. 2005; Gisiger 2001*). Self organised units can maintain activities of multiple units without elaborate control structures, and in early stages of evolution, organisms with such self organised units would have a better chance of survival. The scaling exponent of 3/4 is explained by this hypothesis as an evolutionary accident, i.e. the first self organised biological systems exhibited the scaling relationship and the ‘phenotype’ drifted into the population, much like the evolutionary arguments for the prevalence of pentadactyly (*Laurin 1998*) . But the hypothesis fails to account for possible changes by selection in multicellular organisms which evolved elaborate control structures (endocrine systems, for example) (*D. Glazier 2018*) .

1.1.6.3 Thermodynamic Origin Model

Another notable first principle approach for explaining metabolic scaling with mass uses a thermodynamic framework for energy allocation (*Ballesteros et al. 2018*) . The model proposes a balance between energy dissipated as heat and the energy used to maintain metabolism, to explain the relationship between metabolic rate and mass. Akin to von Bertnaffly’s approach, metabolic rate is assumed to be a weighted sum of an isometric (M) and allometric ($M^{2/3}$) mass term. The energy dissipated as heat would scale with surface area, which in turn scales as $M^{2/3}$. The energy used to maintain metabolism scales linearly with mass, with the assumption that the number of cells increases linearly with mass. The weights for the allometric and isometric terms depend on the efficiency of energy consumption and experimentally derivable prefactors. The model fits data from mammalian basal metabolic rates (*McNab 1988*) very well. The model also predicts the convex curvature of the log-log relationship between metabolic rate and mass, in agreement with the findings of (*Kolokotrones et al. 2010; Bueno & López-Urrutia 2014*)

1.1.6.4 Allometric Cascade Model

There are multiple chemical reactions and physiological feedbacks involved in the production and utilisation of ATP. Rolfe and Brown (1997) have reviewed in detail the biochemical processes and enzymatic activities involved in metabolism (*Rolf & G. Brown 1997*). Each step can be considered as a control site for the sum total process of metabolic activity. Each step’s contribution can be characterised by a control coefficient. The allometric cascade model proposes that each step has a power law relationship with mass (*Darveau et al. 2002*). The metabolic rate can then be represented as a weighted sum of the contribution of each step. These steps include intracellular enzymatic reactions, intercellular activity mediated by transporters, exchangers and pumps, organ physiology mediated by endocrine systems, and ecological and evolutionary forces. The allometric model considers a multilevel regulation of metabolic activity, at different levels of organisation, biochemical and physiological. One key advantage of the model is that it explains the different scaling exponents for basal and maximal

metabolic rate, supported by empirical data. There is supporting evidence from exercise physiology in humans for this model (*Batterham & A. S. Jackson 2003*).

There were similar hypotheses considering multilevel regulation with finite number of levels proposed independent of the allometric cascade model. The three compartment model (*Painter 2005*) considers the effects of scaling at the cellular level, from skin tissues with an exponent of 2/3 and finally from skeletal tissues with an exponent of 1. Another model used five compartments to explain scaling in mammals (*Wang et al. 2001*).

1.1.6.5 Metabolic Level Boundary Hypothesis

The Metabolic Level Boundary Hypothesis (MLBH) is a contextual framework for explaining and predicting metabolic scaling exponents (*D. S. Glazier 2008*). The key arguments of this hypothesis are that (1) the metabolic scaling exponent is constrained by physical and geometrical properties of the organism. (2) The metabolic rate (L) at the geometric mean of the mass range of a set of organisms is a key predictor for the metabolic scaling exponent. (3) Intrinsic and extrinsic factors, such as physiological state and temperature influence L, and therefore, the metabolic scaling exponent. The hypothesis posits that L, the ‘metabolic level’ modulates the influence of surface area and resource demand related processes on metabolic activity. Glazier states that the hypothesis captures variations in the allometric relationship better than previous models, and that MLBH allows for ‘if, then’ predictions (*D. S. Glazier 2010*). A relationship between the metabolic level and metabolic scaling exponent, once established can be used as a predictor for the exponent, given the metabolic level. This hypothesis highlights the point that the metabolic scaling exponent is context dependent, and that a lot of factors affect it. But, it is important to note that the framework does not provide a mechanistic explanation of how different factors affect the metabolic scaling exponent. This hypothesis forms a link between ecology and physiology, and potentially applies to all taxa.

1.2 Shifts in Perspective on Metabolic Scaling

The study of allometric scaling of metabolic activity has come a long way since Rubner’s study in 1883. There have been major shifts in perspective about the value of the scaling exponent, and the possible physical basis for such a relationship. Although models like those of West, Brown and Enquist strongly advocated for the existence of a single allometric scaling exponent of 0.75, large scale statistical analyses of empirical data points against this narrow minded approach. Instead of attempting to explain the scaling as a consequence of a single physical/biological phenomenon, recent models agree that the relationship between metabolic rate and mass depends on multiple factors, depends on the context, developmental stage, life history, nutritional history and environmental factors (*D. Glazier 2018; Packard 2015*). The convex curvature relationship between metabolic activity and mass on a log-log scale also indicates that a power law may not even be the appropriate fit to use (*Kolokotrones et al. 2010; Bueno & López-Urrutia 2014*). Recent hypotheses like the MBLH also attempt to use and explain the intercept of the metabolic rate - mass relationship in their models.

An empirical relationship with such consistency across the scale of life is difficult to overlook. Metabolism being the ‘fire of life’ (*Kleiber et al. 1961*), such a relationship would have far reaching impacts on every level of the ecosystem. The Metabolic Theory of Ecology (MTE) aims to use the allometric scaling of metabolic activity to explain other emergent features of biological structure and dynamics across levels of organization (*J. H. Brown 2004; J. Brown 2016*). In other words, the MTE tries to link metabolic scaling at the individual level to ecosystem phenomenon.

A $3/4$ exponent dependence of metabolic rate with mass, and a Boltzmann type relationship with temperature ($I = I_0 M^{3/4} e^{-E/kT}$) is used as a rule of thumb. Given that metabolic activity is a sum of chemical reactions, the Arrhenius type Boltzmann relationship with temperature is invoked.

Using metabolic rate scaling, the allometric scaling of the following are predicted by the MTE: rate of molecular evolution, individual biomass production, survival and mortality, population growth rates, population densities, species diversity with temperature (*J. F. Gillooly et al. 2001*), energy flux and total biomass production, and trophic dynamics (numbers and mass across food chain). These predictions are also supported by empirical studies (*J. H. Brown 2004*)

1.3 Why is it so complex?

A barrage of hypotheses and explanations have been proposed over the past 50 years to explain the universally observed allometric scaling of metabolic activity (*D. Glazier 2018; White & Kearney 2014; Kearney & White 2012*). These hypotheses invoke various features of the organisms and fundamentals of metabolism in their explanations. These models can be categorised into 4 overarching themes; Surface Area, System Composition, Resource Demand, and Resource Transport (*D. Glazier 2018*). In addition, some hypotheses attempt to link this scaling to emergent ecological phenomenon (*O'Connor et al. 2007*). Many of these hypotheses fall short in explaining current trends and outliers (*Kearney & White 2012*). In my opinion, the larger goal of all these hypotheses has been to come up with a *first principle* explanation for the observed scaling. Leaving aside untestable hypotheses, the most disturbing constraint constraining all these hypotheses has been the lack of thorough experimental evidence (*Kearney & White 2012*). Most of the collected data for metabolic scaling has been empirical (*Kearney & White 2012; D. Glazier 2018*). The conditions under which measurements have been made across such empirical studies are widely different (*Makarieva et al. 2008*). It is important to understand that the principles being observed may not hold true in other species/classes of organisms (*Economos 1979*). These observed principles could very well be effects of more general and fundamental principles. To be able to make that distinction, testing the proposed hypotheses **need** experimentally manipulable model systems, with significant variation in mass, and tools to efficiently, consistently, and accurately probe metabolic activity, and associated parameters. Rather than attempting to explain the exponent as a single value, the ongoing effort should be directed towards explaining why the exponent changes contextually the way it does.

1.4 Experimental Studies on Metabolic Scaling

There are very few instances of experimental studies for exploring allometric scaling of metabolic rates.

In 2017, Burgess et al. reviewed studies on metabolic scaling in modular animals; structural organisms made of repeated morphological units (*Burgess et al. 2017*). Each unit is capable of acquiring, processing, and sharing resources. Colonial cnidarians, bryozoans, and colonial ascidians are examples of modular organisms. Modular organisms allow for indeterminate growth; the variation in mass can be huge, and being composed of independent units, their size and shape is experimentally manipulable. They exhibit a variety of strategies for storing, distributing, and using acquired resources (*Blackstone & Bridge 2005*). These animals had previously been proposed as useful models for distinguishing among competing theories for allometric scaling of metabolic rate. The very first studies indicated isometric scaling of metabolic activity with mass, in the marine bryozoan *Electra pilosa* (*Hughes & Huges 1986*). Of the 11 studies till 2017, from 16 modular animal species, the median estimate of the scaling exponent was 0.79 (*Burgess et al. 2017; Nakaya et al. 2005*).

It remains to be seen what greater insights modular organisms provide towards understanding the allometric scaling of metabolic activity.

In 2019, Thommen et al. used the planarian *Schmidtea mediterranea* to show that body size dependent energy storage is responsible for the 3/4 scaling exponent for metabolic activity in planarians (*Thommen et al. 2019*). On starving, the planarian *Schmidtea* grow when fed and shrink when starved, reversibly. The body length can fluctuate between 0.5mm and 20mm, i.e. a variation of close to 2 orders of magnitude. Micro-calorimetry of the planaria over 24 hour periods were used to estimate metabolic activity. The scaling exponent was found to be 0.75 ± 0.01 . RNAi tools are well established for the planarian *Schmidtea mediterranea*. Their life histories and nutritional histories can be controlled and experimentally manipulated. These advantages make the planaria a promising model for studying the physical bases of metabolic scaling.

Although the aforementioned experimental model systems are fascinating and have the potential to provide useful insights, the variation in size is still low. Modular animals do not have suitable molecular tools established for genetic manipulations. There is little control over the life histories of these organisms. The size variation in planaria is less than 2 orders of magnitude (*Thommen et al. 2019*). In the next chapter, I propose the experimentally evolved snowflake yeast (*Ratcliff & Travisano 2014*), which shows a variation of over 6 orders of magnitude in size, as a possible experimental model system for studying the allometric scaling of metabolic activity.

References

1. Agutter, P. S. & Tuszynski, J. A. Analytic theories of allometric scaling, 1055–1062 (2011).
2. Agutter, P. S. & Wheatley, D. N. Metabolic scaling: Consensus or controversy? *Theoretical Biology and Medical Modelling* **1**, 1–11. ISSN: 17424682 (2004).

3. Altman, P. & Dittmer, D. Metabolism. Bethesda. *Maryland: Federation of American Societies for Experimental Biology* (1968).
4. Ballesteros, F. J. *et al.* On the thermodynamic origin of metabolic scaling. *Scientific Reports* **8**. ISSN: 20452322. doi:10.1038/s41598-018-19853-6. arXiv: 1407.3659 (Dec. 2018).
5. Banavar, J. R., Damuth, J., Maritan, A. & Rinaldo, A. Supply{\textendash}demand balance and metabolic scaling. *Proceedings of the National Academy of Sciences* **99**, 10506–10509 (2002).
6. Banavar, J. R., Moses, M. E., *et al.* A general basis for quarter-power scaling in animals. *Proceedings of the National Academy of Sciences of the United States of America* **107**, 15816–15820. ISSN: 00278424 (Sept. 2010).
7. Batterham, A. M. & Jackson, A. S. Validity of the allometric cascade model at submaximal and maximal metabolic rates in exercising men. *Respiratory physiology & neurobiology* **135**, 103–106 (2003).
8. Bertalanffy, L. v. T HE QUARTERLY REVIEW of BIOLOGY. **32**, 333–406 (1949).
9. Blackstone, N. W. & Bridge, D. M. Model Systems for Environmental Signaling1. *Integrative and Comparative Biology* **45**, 605–614. ISSN: 1540-7063 (Aug. 2005).
10. Blum, J. J. On the geometry of four-dimensions and the relationship between metabolism and body mass. *Journal of Theoretical Biology* **64**, 599–601. ISSN: 10958541 (1977).
11. Brody, S. Bioenergetics and Growth, Reinhold Publ. Co., New York, 265–266 (1945).
12. Brown, J. Review : Metabolic ecology : the whole story ? Author (s): Douglas S . Glazier Review by : Douglas S . Glazier Published by : Wiley Stable URL : <http://www.jstor.org/stable/23435693> Accessed : 06-07-2016 19 : 49 UTC Your use of the JSTOR archive indicat. **94**, 263–264 (2016).
13. Brown, J. H. Towards a Metabolic Theory of Ecology. *Robert H MacArthur Award Lecture* **85**, 228–230. ISSN: 0032-4663 (2004).
14. Bueno, J. & López-Urrutia, Á. Scaling up the curvature of mammalian metabolism. *Frontiers in Ecology and Evolution* **2**, 1–13. ISSN: 2296701X (2014).
15. Burgess, S. C. *et al.* Metabolic scaling in modular animals. *Invertebrate Biology* **136**, 456–472. ISSN: 17447410 (2017).
16. Butler, J. P., Feldman, H. A. & Fredberg, J. J. Dimensional analysis does not determine a mass exponent for metabolic scaling. *American Journal of Physiology-Regulatory, Integrative and Comparative Physiology* **253**, R195–R199 (1987).
17. Champy, C. Sexualité et hormones. *Doin, Paris* (1924).
18. Coulson, R. A. Metabolic rate and the flow theory: a study in chemical engineering. *Comparative Biochemistry and Physiology Part A: Physiology* **84**, 217–229 (1986).
19. Da Silva, J. K. L., Garcia, G. J. & Barbosa, L. A. Allometric scaling laws of metabolism. *Physics of Life Reviews* **3**, 229–261. ISSN: 15710645 (2006).
20. Da Silva, J. K., Barbosa, L. A. & Silva, P. R. Unified theory of interspecific allometric scaling. *Journal of Physics A: Mathematical and Theoretical* **40**, F953 (2007).
21. Darveau, C.-A., Suarez, R. K., Andrews, R. D. & Hochachka, P. W. Allometric cascade as a unifying principle of body mass effects on metabolism. *Nature* **417**, 166–170 (2002).
22. Davison, J. Body weight, cell surface, and metabolic rate in anuran Amphibia. *The Biological Bulletin* **109**, 407–419 (1955).
23. Dodds, P. S., Rothman, D. H. & Weitz, J. S. Re-examination of the "3/4-law" of metabolism. *Journal of Theoretical Biology* **209**, 9–27. ISSN: 00225193 (Mar. 2001).

24. Dubois, E. Sur le rapport du poids de l'encéphale avec la grandeur du corps chez les mammifères. *Bulletins et Mémoires de la Société d'Anthropologie de Paris* **8**, 337–376 (1897).
25. Economos, A. Gravity, metabolic rate and body size of mammals. *The Physiologist* **22**, S71–2 (1979).
26. Gardner, J. D., Laurin, M. & Organ, C. L. The relationship between genome size and metabolic rate in extant vertebrates. *Philosophical Transactions of the Royal Society B* **375**, 20190146 (2020).
27. Gillooly, J. F., Brown, J. H., West, G. B., Savage, V. M. & Charnov, E. L. Effects of size and temperature on metabolic rate. *Science* **293**, 2248–2251. ISSN: 00368075 (2001).
28. Ginzburg, L. & Damuth, J. The space-lifetime hypothesis: Viewing organisms in four dimensions, literally. *American Naturalist* **171**, 125–131. ISSN: 00030147 (2008).
29. Gisiger, T. Scale invariance in biology: coincidence or footprint of a universal mechanism? *Biological Reviews* **76**, 161–209 (2001).
30. Glazier, D. Metabolic Scaling in Complex Living Systems. *Systems* **2**, 451–540. ISSN: 2079-8954 (2014).
31. Glazier, D. Rediscovering and Reviving Old Observations and Explanations of Metabolic Scaling in Living Systems. *Systems* **6**, 4. ISSN: 2079-8954 (Jan. 2018).
32. GLAZIER, D. S. The 3/4-Power Law Is Not Universal: Evolution of Isometric, Ontogenetic Metabolic Scaling in Pelagic Animals. *BioScience* **56**, 325. ISSN: 0006-3568 (2006).
33. Glazier, D. S. A unifying explanation for diverse metabolic scaling in animals and plants. *Biological Reviews* **85**, 111–138. ISSN: 14647931 (2010).
34. Glazier, D. S. *Beyond the '3/4-power law': Variation in the intra- and interspecific scaling of metabolic rate in animals* Nov. 2005. doi:10.1017/S1464793105006834.
35. Glazier, D. S. Effects of metabolic level on the body size scaling of metabolic rate in birds and mammals. *Proceedings of the Royal Society B: Biological Sciences* **275**, 1405–1410 (2008).
36. Gould, S. J. Allometry and size in ontogeny and phylogeny. *Biological reviews of the Cambridge Philosophical Society* **41**, 587–640. ISSN: 00063231 (1966).
37. Gregory, T. R. The bigger the C-value, the larger the cell: genome size and red blood cell size in vertebrates. *Blood Cells, Molecules, and Diseases* **27**, 830–843 (2001).
38. Gunther, B. Dimensional analysis and theory of biological similarity. *Physiological Reviews* **55**, 659–699 (1975).
39. Heusner, A. A. Energy metabolism and body size II. Dimensional analysis and energetic non-similarity. *Respiration Physiology* **48**, 13–25. ISSN: 00345687 (1982).
40. Hill, A. The series elastic component of muscle. *Proceedings of the Royal Society of London. Series B, Biological Sciences*, 273–280 (1950).
41. Hochachka, P. W. & Somero, G. N. *Biochemical adaptation: mechanism and process in physiological evolution* (Oxford University Press, 2002).
42. Hughes, D. J. & Huges, R. N. Metabolic Implications of Modularity: Studies on the Respiration and Growth of Electra pilosa. *Philosophical Transactions of the Royal Society of London Series B* **313**, 23–29 (Aug. 1986).
43. Hui, D. & Jackson, R. B. Uncertainty in allometric exponent estimation: a case study in scaling metabolic rate with body mass. *Journal of Theoretical Biology* **249**, 168–177 (2007).

44. Isaac, N. J. & Carbone, C. Why are metabolic scaling exponents so controversial? Quantifying variance and testing hypotheses. *Ecology letters* **13**, 728–735 (2010).
45. Kearney, M. R. & White, C. R. Testing metabolic theories. *American Naturalist* **180**, 546–565. ISSN: 00030147 (2012).
46. Kleiber, M. *BODY SIZE AND METABOLIC RATE* tech. rep. (1947), 1947.
47. Kleiber, M. *et al.* Body size and metabolism. *Hilgardia* **6**, 315–353 (1932).
48. Kleiber, M. *et al.* The fire of life. An introduction to animal energetics. *The fire of life. An introduction to animal energetics.* (1961).
49. Kolokotrones, T., Van Savage, Deeds, E. J. & Fontana, W. Curvature in metabolic scaling. *Nature* **464**, 753–756. ISSN: 00280836 (Apr. 2010).
50. Kooijman, B. & Kooijman, S. *Dynamic energy budget theory for metabolic organisation* (Cambridge university press, 2010).
51. Kozłowski, J. & Konarzewski, M. *West, Brown and Enquist's model of allometric scaling again: the same questions remain* tech. rep. (2005).
52. Kozłowski, J., Konarzewski, M. & Gawelczyk, A. Cell size as a link between noncoding DNA and metabolic rate scaling. *Proceedings of the National Academy of Sciences* **100**, 14080–14085 (2003).
53. Kozłowski, J. & Weiner, J. *INTERSPECIFIC ALLOMETRIES ARE BY-PRODUCTS OF BODY SIZE OPTIMIZATION* tech. rep. 2 (1997), 352–380. <<http://www.journals.uchicago.edu/t-and-c>>.
54. Krebs, H. Body size and tissue respiration. *Biochimica et biophysica acta* **4**, 249–269 (1950).
55. Lasiewski, R. C. & Dawson, W. R. A re-examination of the relation between standard metabolic rate and body weight in birds. *The Condor* **69**, 13–23 (1967).
56. Laurin, M. A reevaluation of the origin of pentadactyly. *Evolution* **52**, 1476–1482 (1998).
57. Maino, J. L., Kearney, M. R., Nisbet, R. M. & Kooijman, S. A. Reconciling theories for metabolic scaling. *Journal of Animal Ecology* **83**, 20–29. ISSN: 00218790 (2014).
58. Makarieva, A. M. *et al.* Mean mass-specific metabolic rates are strikingly similar across life's major domains: Evidence for life's metabolic optimum. *Proceedings of the National Academy of Sciences of the United States of America* **105**, 16994–16999. ISSN: 00278424 (2008).
59. McMahon, T. Size and shape in biology: elastic criteria impose limits on biological proportions, and consequently on metabolic rates. *Science* **179**, 1201–1204 (1973).
60. McNab, B. K. Complications inherent in scaling the basal rate of metabolism in mammals. *Quarterly Review of Biology* **63**, 25–54. ISSN: 00335770 (1988).
61. Nakaya, F., Saito, Y. & Motokawa, T. Experimental allometry: effect of size manipulation on metabolic rate of colonial ascidians. *Proceedings of the Royal Society B: Biological Sciences* **272**, 1963–1969 (2005).
62. O'Connor, M. P. *et al.* Reconsidering the mechanistic basis of the metabolic theory of ecology. *Oikos* **116**, 1058–1072. ISSN: 0030-1299 (2007).
63. Packard, G. C. Quantifying the curvilinear metabolic scaling in mammals. *Journal of Experimental Zoology Part A: Ecological Genetics and Physiology* **323**, 540–546. ISSN: 19325231 (2015).
64. Painter, P. R. Data from necropsy studies and in vitro tissue studies lead to a model for allometric scaling of basal metabolic rate. *Theoretical Biology and Medical Modelling* **2**, 1–8. ISSN: 17424682 (2005).

65. Patterson, M. R. A mass transfer explanation of metabolic scaling relations in some aquatic invertebrates and algae. *Science* **255**, 1421–1423 (1992).
66. Prothero, J. Methodological aspects of scaling in biology. *Journal of Theoretical Biology* **118**, 259–286 (1986).
67. Ratcliff, W. C. & Travisano, M. *Experimental evolution of multicellular complexity in saccharomyces cerevisiae* 2014. doi:10.1093/biosci/biu045.
68. Rolf, D. & Brown, G. Cellular energy utilization and molecular origin of standard metabolic rate in mammals. *Physiol. Rev* **77**, 731–756 (1997).
69. Rubner, M. *Der energiewert der Kost des Menschen* (1883).
70. Sarrus, F. Sarrus and Rameaux, 1838, translated into 365 English by R. Shour. *ResearchGate* **366** (2017).
71. Savage, V. M., Gillooly, J. F., et al. The predominance of quarter-power scaling in biology tech. rep. (2004), 257–282.
72. Savage, V. M., Deeds, E. J. & Fontana, W. Sizing up allometric scaling theory. *PLoS Computational Biology* **4**. ISSN: 1553734X. doi:10.1371/journal.pcbi.1000171 (Sept. 2008).
73. Seeherman, H. J., Taylor, C. R., Maloy, G. M. & Armstrong, R. B. Design of the mammalian respiratory system. II. Measuring maximum aerobic capacity. *Respiration physiology* **44**, 11–23 (1981).
74. Szarski, H. Changes in the amount of DNA in cell nuclei during vertebrate evolution. *Nature* **226**, 651–652 (1970).
75. Thommen, A. et al. Body size-dependent energy storage causes Kleiber's law scaling of the metabolic rate in planarians. *eLife* **8**, 1–69. ISSN: 2050084X (2019).
76. Thompson, D. *On growth and form* 1942.
77. Van der Meer, J. Metabolic theories in ecology. *Trends in ecology & evolution* **21**, 136–140 (2006).
78. Von Bertalanffy, L. Quantitative laws in metabolism and growth. *The quarterly review of biology* **32**, 217–231 (1957).
79. Wang, Z., O'Connor, T. P., Heshka, S. & Heymsfield, S. B. The reconstruction of Kleiber's law at the organ-tissue level. *The journal of nutrition* **131**, 2967–2970 (2001).
80. West, D. & West, B. J. Physiologic time: A hypothesis. *Physics of Life Reviews* **10**, 210–224. ISSN: 15710645 (2013).
81. West, G. B., Brown, J. H. & Enquist, B. J. A general model for the origin of allometric scaling laws in biology. *Science* **276**, 122–126. ISSN: 00368075 (1997).
82. West, G. B., Brown, J. H. & Enquist, B. J. The fourth dimension of life: Fractal geometry and allometric scaling of organisms. *Science* **284**, 1677–1679. ISSN: 00368075 (1999).
83. White, C. R. & Kearney, M. R. Metabolic scaling in animals: Methods, empirical results, and theoretical explanations. *Comprehensive Physiology* **4**, 231–256. ISSN: 20404603 (2014).
84. Witting, L. Body mass allometries caused by physiological or ecological constraints? *Trends in Ecology & Evolution* **13**, 25. ISSN: 01695347 (1998).

Chapter 2

The Snowflake Yeast

Multicellularity is one of the major transitions in evolution that allowed for increased complexity. It is the integration of ‘previously autonomous cells into new, more complex organisms’ (*Rebolleda-Gómez et al. 2016*). There are many questions that remain about how the transition from unicellular organisms to multicellular organisms may have occurred. It is possible that formation of clonally developing clusters is the first step towards multicellularity (*Bonner 1998*). In 2012, Ratcliff et al. described a yeast based system for studying higher level evolvability and the origins of multicellularity (*Ratcliff, Denison, et al. 2012*). They showed that disruption of a single transcription factor, *ACE2*, generates a ‘multicellular’ variant of yeast. This variant, the snowflake yeast suggests that simple microevolutionary changes ($\Delta ACE2$) can have profound macroevolutionary consequences (multicellularity) (*Ratcliff, Denison, et al. 2012; Ratcliff, Fankhauser, et al. 2015*).

The snowflake yeast is derived from the Y55 strain of yeast. A population is subjected to a settling selection, by allowing a culture to settle on a bench for a period of time, after which the lower 100 μl is aliquoted to subculture the next generation (*Ratcliff, Denison, et al. 2012*). The subculture is allowed to grow for 24 hours, after which the selection protocol is repeated. This selection process was continued for over 400 transfers. The resulting snowflake volumes after the transfers vary across 6 orders of magnitude in size. Comparing gene expressions between the wild-type yeast and the evolved populations showed that expression of a total of 143 genes differed by more than 2 fold. Of the 10 most down-regulated genes, 7 were involved in the separation of the daughter cell after division. These 7 genes are regulated by the transcription factor *ACE2* (*Ratcliff, Fankhauser, et al. 2015*).

One of the fundamental questions in the philosophy of biological individuality, and organismality is about when a cluster of cells can be defined as a multicellular *individual*. Definitions that may work for plants and animals may not be applicable for organisms at the interface of multicellularity (*Herron et al. 2013*). One of the consensus in that a cluster can be classified as an individual when it is capable of evolving under Darwinian principles, as a whole. Specifically, the individuals should have heritable variation, which affects fitness (*Godfrey-Smith 2011*). Ratcliff et. al., in using their sedimentation rate selection paradigm, showed that the yeast snowflake can indeed be characterized as an individual under this definition (*Ratcliff, Fankhauser, et al. 2015; Ratcliff & Travisano 2014*).

Given that whole clusters settle under selection and are propagated, or fail to do so and are wiped out, the clusters can be considered *units of selection*. The snowflake size is heritable. Clusters from the same clone have similar physiological properties; growth form, cell-cell adhesive growth, cell size and shape. Comparing parent-offspring cultures, Ratcliff et. al. calculated the heritability of size at 0.84 (*Ratcliff, Fankhauser, et al. 2015*). The snowflake yeast break at cell-cell connection when they split. This creates a genetic bottleneck when producing daughter snowflakes. Cell-cell connections can be broken between combinations of mutant or wild type cells. At the break, all cells in the snowflake would be descended from a single cell. This genetic bottleneck allows for reduced genetic conflict within the snowflake (*Ratcliff, Fankhauser, et al. 2015*) This feature separates a snowflake from a mere cluster of cells. That the individual snowflakes, if sheared, grow to nearly the same characteristic size being selected for, even in the absence of the selection pressure indicates that the cluster isn't a result of self-organization. The size of the snowflake is limited by fracture-inducing internal stress (*Jacobeen, Graba, et al. 2018*).

2.1 Appeal as a Model System for Metabolic Scaling

The aspect of this model system that is relevant to the quest towards understanding metabolic scaling is the variation in size that the snowflake is capable of exhibiting. The genetic tools available for *Saccharomyces cerevisiae* provides significant potential for studying allometric scaling of metabolic rates (*Duina et al. 2014*). For context, the planarian model system used by Thommen et al, as described in Chapter 1 has a mass variation of less than 2 orders of magnitude (*Thommen et al. 2019*). The yeast snowflake can be selected for a size variation of over 6 orders of magnitude. Being a yeast based system, the genetic similarity across the snowflakes, metabolic scaling studies on the snowflake can be categorized as intraspecific studies. As an experimentally evolved system, the yeast snowflake also allow for control over the evolutionary history, life history and ontogeny of the snowflake.

In 2014, Glazier classified hypotheses and theories proposed for explaining the scaling exponent into 4 categories on the basis of their approach; Surface Area, System Composition, Resource Demand, and Resource Transport (*Glazier 2014*). The genetic tools available in yeast allows can allow for manipulations suitable for each of these approaches. The snowflake yeast has the potential to be used as a model system to test most existing hypotheses for metabolic scaling.

2.2 Characterization of the Model System

The Ratcliff Lab, where the snowflake populations were evolved, were gracious enough to send the Thutupalli Lab at NCBS, 8 populations of the snowflake yeast. These were obtained after 8, 21, 50, 100, 145, 200, 300 and 400 repetitions of the transfer protocol described in the previous section. To maintain the populations in the lab, the same selection protocol was continued, but with varying sedimentation times (provided in Table 1) (*personal communication*).

The yeast snowflake seems to be an exciting model system for studying allometric scaling of metabolic activity. However, to be able to co-opt it for such an endeavor involves some characterization.

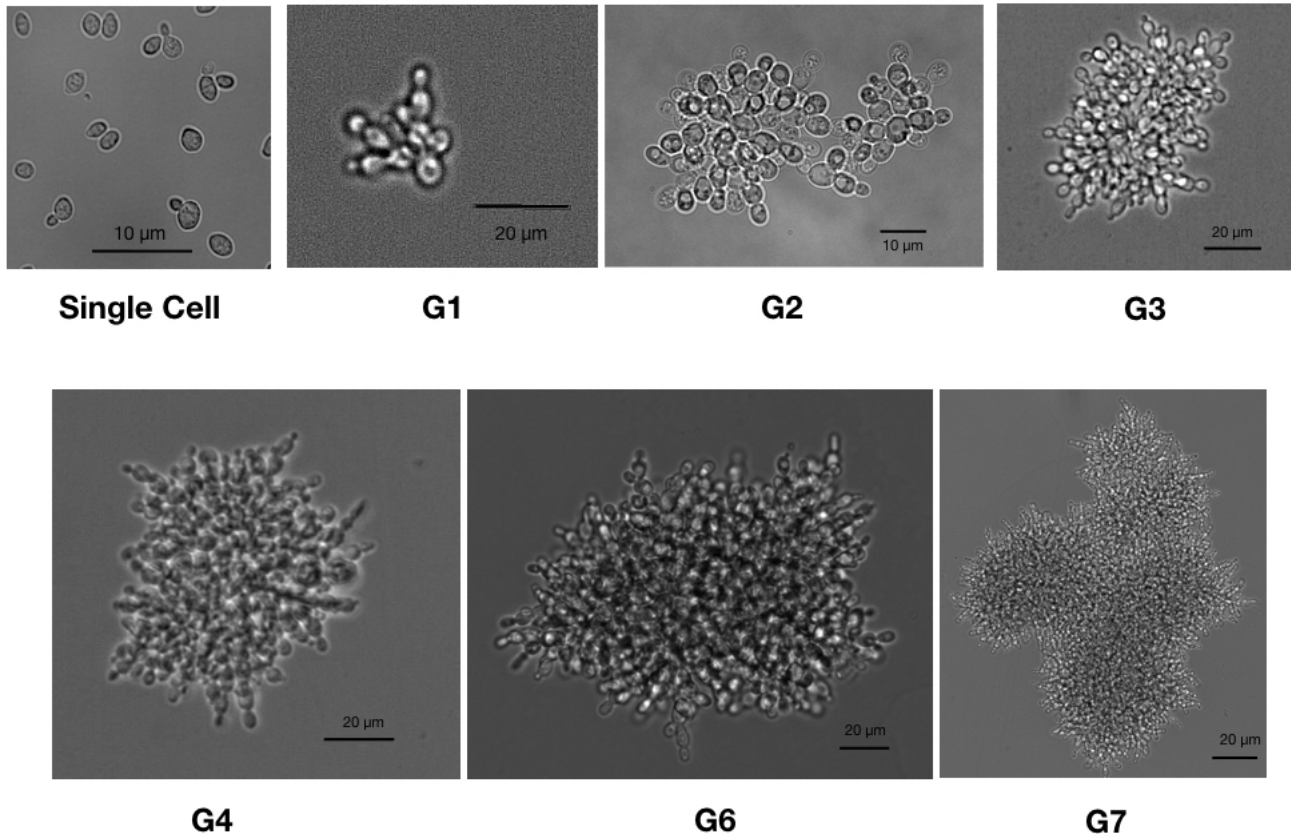


Figure 2.1: Images of different populations of the snowflake yeast. The selection protocol for these populations are given in Table1. Note that G7 has more elongated cells than the other populations

While making population level measurements of metabolic activity from the yeast snowflakes, it is important to know the distribution of the masses and sizes of the snowflake yeast culture. Appropriate time points must be chosen where the intra-culture variation is minimal. In a culture in stationary phase, there is a significant spread in cluster sizes, owing to the presence of juvenile, adult and dividing snowflakes. Additionally, to ensure that ‘metabolic state’ is similar across measurements, the snowflakes must be in a phase analogous to the exponential growth period in unicellular yeast.

A method to probe and characterize this population level variance over time is to start with a synchronized system. All the individuals at this point should be homogeneous. One way to enforce this, is to start with a culture of single cells derived from the snowflake. It is known from literature that each cell would grow to the characteristic size of the snowflake and then split (Ratcliff 2014b).

Physical forces which can shear the snowflake does not separate the snowflake into single cells. The *ACE2* mutation that is characteristic to the yeast snowflake regulates the gene *CTS1*, which transcribes an endochitinase enzyme (Ratcliff, Fankhauser, et al. 2015). In the wild type yeast, this enzyme can break the cell-cell adhesion. If the enzyme were to be provided externally, the yeast snowflake could be deconstructed into single cells. But, it is important to note that excessive chitinase treatment can lead to cell lysis (*personal communication*).

Population Name	Number of Transfers	Selection: Sedimentation Time	Chitinase Action Time
G1	8	120s	-
G2	21	120s	12 hours
G3	50	90s	10.5 hours
G4	100	60s	9.5 hours
G5	145	45s	9.5 hours
G6	200	30s	-
G7	300	20s	-
G8	400	10s	-

Table 2.1: Details of selection, maintainence and chitinase action for the different populations of snowflakes used

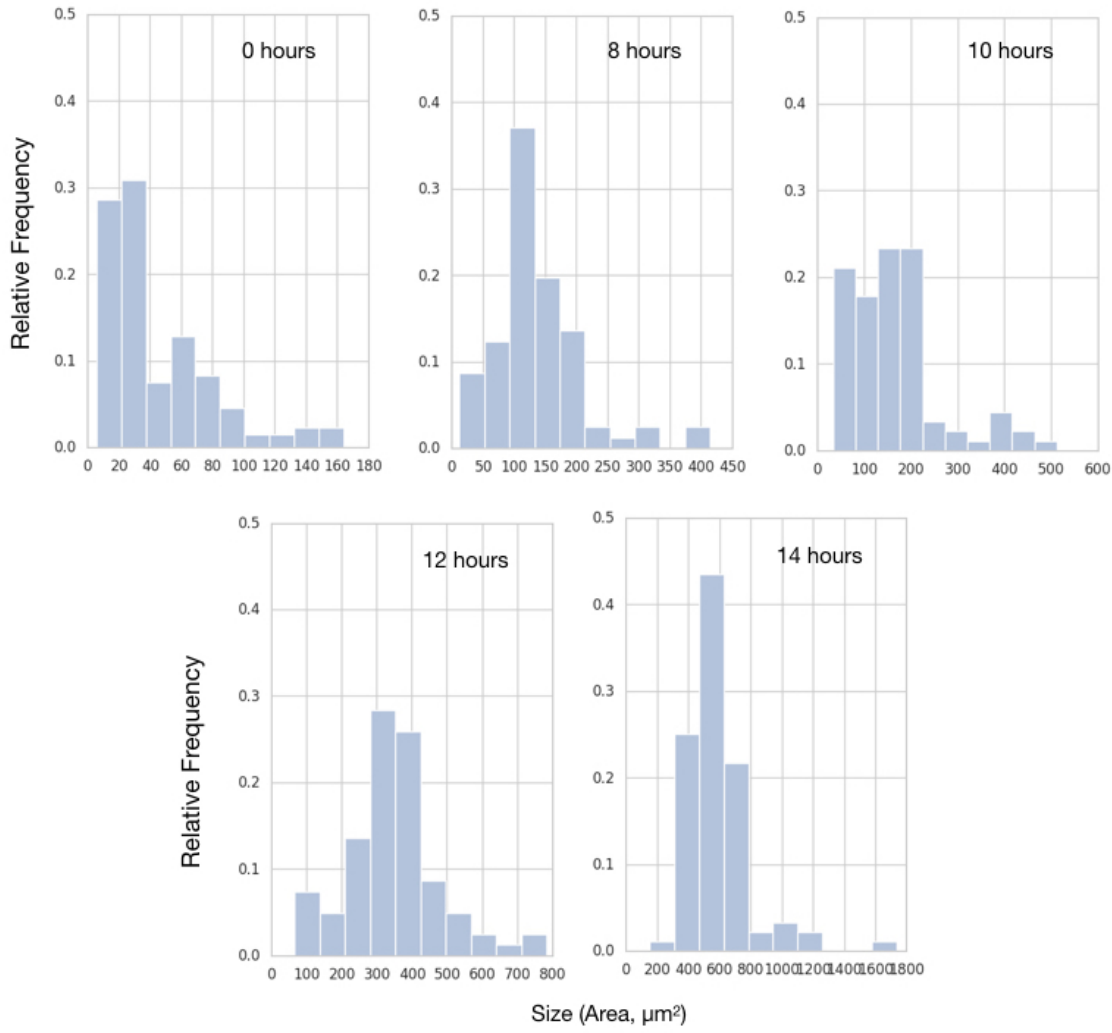


Figure 2.2: Time series of size distributions of a snowflake after chitinase action. The protocol is described in the text. Note that the variation is least at 14 hours.

First, the duration of the chitinase treatment for the snowflake populations had to be standardized. It was found that 1 g/L chitinase added to the snowflake culture, while being stirred at 300 rpm, in a 30°C incubator was most appropriate. 1g/L Chitinase (Sigma) was prepared in 50mM potassium phosphate buffer at pH 6.0, and stored at -20°C (*Ratcliff Lab, personal communication*). The duration of chitinase treatment, such that only single cells remained in the culture varied according to the size of the snowflake. For G2, 12 hours; G3, 11 hours; G4 and G5, 9.5 hours. G6, G7 and G8 could not be characterized in the duration of this project.

From single cells, the growth rates of the snowflake populations could be characterized. The synchronized single cell culture was tracked for size and number of snowflakes to generate growth curve. After treatment with chitinase, the culture is aliquoted into 4 tubes containing 5ml of YPD media. After a set period of time, the culture is mixed well, and 50 μ l is dropped on a slide. A cover slip is gently placed over the drop. Images of the entire region under the coverslip are captured under a microscope. This process is done for 4 pre-determined time points, depending on the population. The images are thresholded and the area of each snowflake in the image is calculated using ImageJ (*Schindelin et al. 2012*). The distribution of the sizes of clusters in the culture is compared to identify the best time point to use for further experiments, i.e. where the distribution is the tightest. Figure 2.2 shows one such histogram time series for G2. Note that for G2, at 14 hours, the size distribution peaks close to $600 \mu\text{m}^2$. The appropriate times are identified for G3, G4 and G5 using the same protocol. Figure 2.3 shows the size distribution in the populations at the identified times. As expected, the size increases monotonically with the populations. The variation also increases.

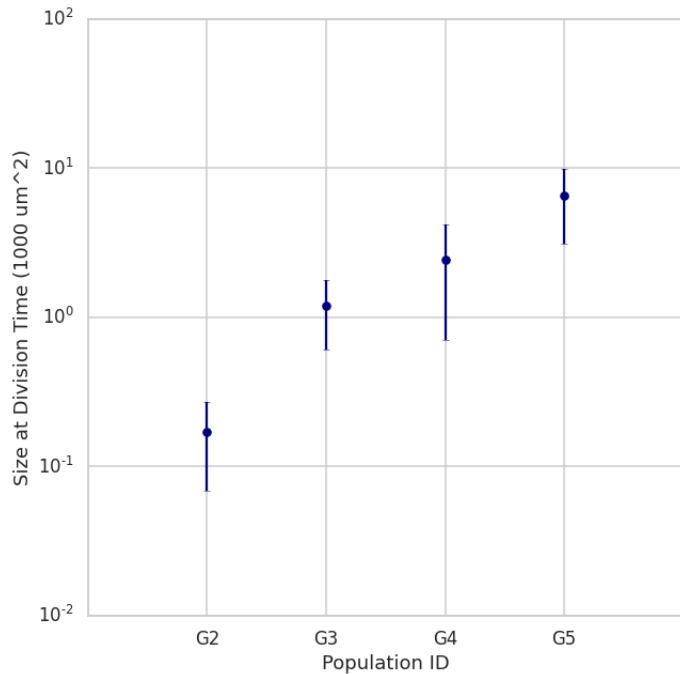


Figure 2.3: Size of the yeast snowflake of different populations at the timepoint where the size distributions were the tightest. Note that G6, G7, G8 have not been analysed. With these populations, the size variation across the plot would be higher. Also, the area of the top view of the snowflake is being plotted on the Y Axis

2.3 Measuring Mass of the Snowflakes

The current state of the art technique for measuring mass from single cells or cellular aggregates is the suspended micro-channel resonator method (*Łabędż et al. 2017*). The SMR is made of a silicon cantilever, with an embedded microfluidic channel. The cantilever oscillates at a frequency proportional to its mass. If a cell passes through the channel, the total mass at the cantilever changes, thereby changing the frequency of oscillation. The cantilever frequency response is optically detected, and the mass of the flowing cell can be estimated (*Grover et al. 2011*). This protocol has been characterized for single cells of yeast, and bacteria (*Popescu et al. 2014*). For larger aggregates, like a snowflake, custom made silicon cantilevers, with large enough microfluidic channels would have to be designed and fabricated. Additionally, the optical sensors associated with the device would have to be carefully set up and calibrated. Given the variation in sizes, multiple such devices would have to be made and set-up. Although theoretically feasible, time constraints associated with this project dissuaded implementation of the state of the art approach. Instead, a much more basic, rudimentary method has been adopted to estimate mass.

2.3.1 Filter Technique

In a report from 1989, Does and Bisson describe a simple, elegant method for measuring mass from a population of cells (*Does & Bisson 1989*). A known volume of a culture of cells is passed through a filter, whose mass is known. The filter is dried in an oven, and the mass of the dried cellular material is estimated. The number of cells can be calculated by estimating CFUs, or flow cytometry (*Vembadi et al. 2019*). With the total cellular dry mass and the number of cells, the mass per cell can be estimated.

I attempted this method for measuring the mass of *Cen.PK* yeast cells as a proof of concept for the snowflake mass measurement. A $0.22\text{ }\mu\text{m}$ filter was weighed M_1 on a balance with a least count of 0.1mg . 10ml of a yeast *Cen.PK* culture in mid-exponential phase was passed through the filter. It is assumed that the dead cell debris contributes very little to the biomass during this phase. The filter was then kept in a $70\text{ }^{\circ}\text{C}$ oven for 6 hours for drying. I found that between 6 hours to 24 hours in the oven, the filter mass does not change more than 0.1 mg (least count of balance). The filter is weighed again, to obtain M_2 . Immediately before the 10ml culture is passed through the filter, different dilutions of the culture were spread on a YPD-agar plate for obtaining CFU counts to estimate the number density of cells in the culture. Using this information, the total number of cells N passed through the filter is estimated. Assuming homogeneity among cells, the mass of each cell is therefore $M_c = (M_2 - M_1)/N$.

To ensure that the method gives consistent results, different dilutions of the *Cen.PK* culture were used to estimate mass in triplicates. Figure 4 confirms that the masses obtained from these dilutions of the same culture match.

The estimated mass of the yeast cell from this method is **$40.7 \pm 1.9\text{ pg}$** . From SMR measurements on yeast, masses were estimated to be $47.65 \pm 1.05\text{ pg}$ (*Łabędż et al. 2017*).

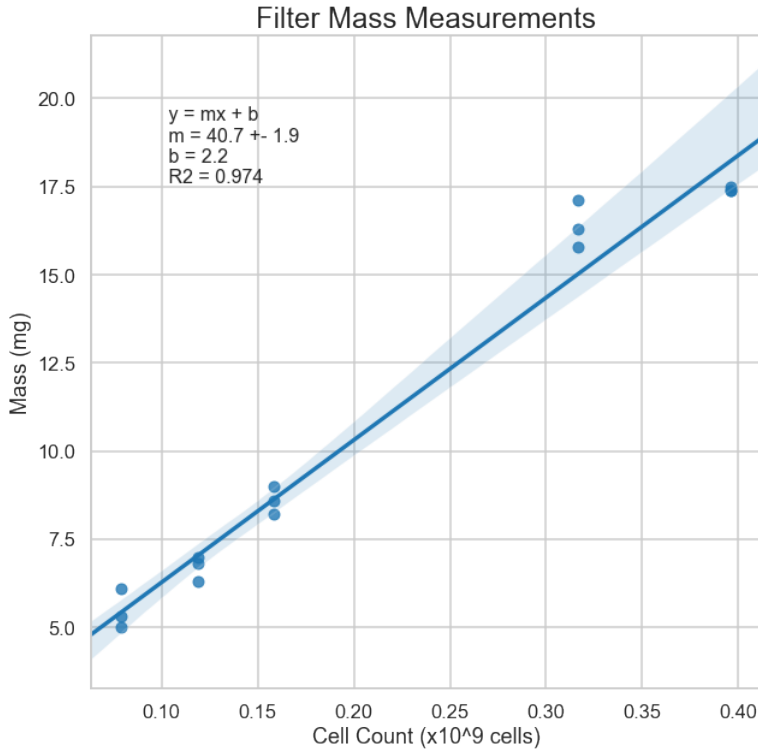


Figure 2.4: Characterising the filter method for mass measurement. Different dilutions of the same culture of yeast cells were used to estimate mass. The mass difference $M_2 - M_1$ (see text) is plotted against the dilution factor.

2.3.2 Volume and Density

Mass can be measured indirectly by combining accurate measurements of density and volume. Volumes can be estimated using confocal microscopy (*Model 2018*). Density gradient centrifugation can be co-opted to measure densities of the yeast snowflakes (*Oliver et al. 1981*).

2.3.2.1 Density Measurement

The sedimentation rate of a particle at a fixed centrifugal force and liquid viscosity is proportional to the size of the particle and the difference in densities of the particle and the liquid. If the density of the particle matches that of the surrounding liquid, the sedimentation rate is zero (*Pertoft et al. 1979*). Percoll is one of the commercially available solutions for generating density gradients. Its properties have been extensively studied (*T. C. Laurent et al. 1980*). It is a polydisperse colloid of silica, sizes ranging from 15 - 20 nm. On centrifugation, the particles' sedimentation rate differs, and depending to the distribution of the particle sizes, a density gradient is set up along the tube.

For making biological measurements in a Percoll gradient, it is important to ensure that the osmolality of the Percoll solution being used matches that of the cells (*T. C. Laurent et al. 1980*). If the cells are put in a non-isotonic solution, their volumes will change, and therefore their densities. The Sigma Aldrich handbook for Percoll recommends adding 9 parts of Percoll to 1 part of 1.5M NaCl, by

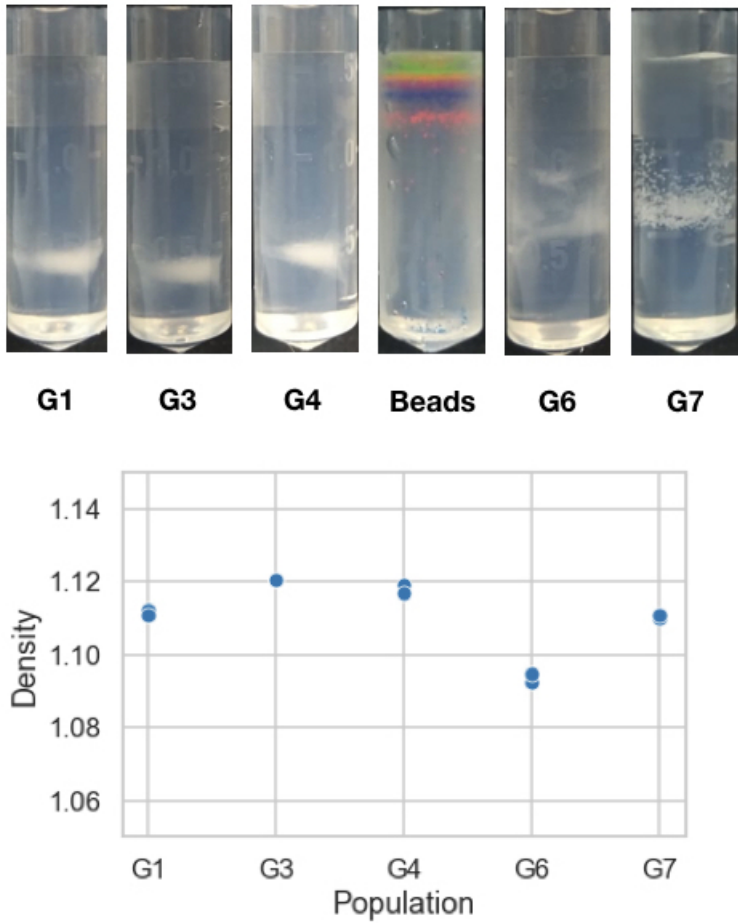


Figure 2.5: Densities of the snowflake populations estimated from Percoll based Density Gradient Centrifugation. Coloured density bead markers are used for calibrations. The densities vary across populations.

volume to make a stock isotonic Percoll solution (SIP). The density of the total solution can then be further changed by diluting with 0.15M NaCl. The density ranges that can be obtained in the Percoll density gradient depends on the speed of centrifugation, time of centrifugation, and the density of the initial well mixed colloidal Percoll. For the snowflakes, a 90% SIP Percoll solution is aliquoted into 2ml cylindrical vials (Eppendorf), and centrifuged at 20000 rcf for 15 minutes at 4C to generate the density gradient. 100 μ l of the snowflake culture is gently pipetted above the Percoll and centrifuged again at 400rcf for 1 hour. Bands or streaks corresponding to the density are visible at the end of the hour long centrifugation. The density gradient can be quantified by using commercially available density marker beads (*Cospheric*). With this calibration, and the position where the clusters form a band/streak, the density of the clusters can be estimated (Pertoft et al. 1979).

For the yeast snowflake, it was found that the density changes with the population type. G3 is denser than G2 and G4. G6 has the least density, and G7 is as dense as G3 (Figure 5). Theoretical simulations show that cells becoming longer can decrease the rate of internal stress accumulation (Jacobeen, Graba, et al. 2018; Jacobeen, Pentz, et al. 2018), which is responsible for the snowflake splitting. The larger

snowflakes have elongated cells (See Figure 1). The cell-elongation strategy adopted by the larger flakes could explain this non-monotonous change in densities across populations. This observation also negates that the widespread assumption of density being constant, a common feature in most models for explaining metabolic scaling (see Chapter 1)

2.3.2.2 Volume Measurement

1. The Coulter method measures liquid displacement. A conductive fluid is passed through a small aperture. The impedance across the aperture depends on the volume of this conductive fluid in the aperture. If an object were to pass through the aperture, displacing the fluid, the impedance changes. This short term change in impedance can be recorded as a voltage pulse. So, when a cell passes through the compartment, the voltage measured across the circuit spikes (*Don 2003*). Traditionally, such a method has been used to count cells in a Coulter counter. But, analyzing the voltage spike profile can provide details of the total volume that was displaced, and therefore, the cell volume (*Model 2018*). The Coulter principle is one of the fundamental principles used in a flow cytometer (*Vembadi et al. 2019*).
2. Confocal Microscopy can provide depth-sectioned images of the snowflake. Scanning the snowflake at small vertical x steps can provide a series of cross sectional areas, which can then be integrated to estimate the volume. For an object like in Figure 6 with a step size of Δz , and N cross sectional areas A_i , the volume is:

$$V = \sum_{i=1}^N A_i \Delta z$$

The approximation becomes better as Δz becomes smaller (*Errington & White 1999*).

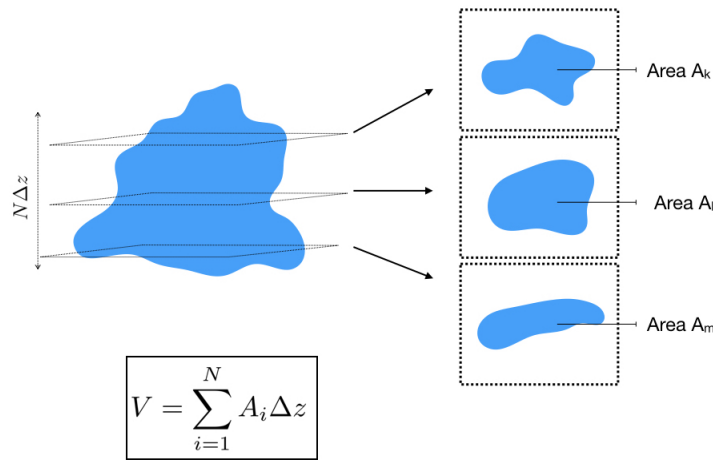


Figure 2.6: Schematic for measuring volume from depth sectioned images

Unfortunately, neither methods for volume measurement could be carried out for the snowflake yeast, or single cells.

2.4 Concluding Statements

The yeast snowflake, originally evolved as a system for studying the origin of multicellularity can be co-opted as an experimental model for studying the allometric scaling of metabolic activity. The genetic tools available in yeast and the size variation of 6 orders of magnitude across the snowflake populations allow for experimental manipulations and measure responses in the metabolic scaling exponent. The G8 population can reach diameters of close to 1mm for each snowflake. The size variation from a single cell to the G8 population spans 6 orders of magnitude. The genetic similarity across the snowflakes imply that the observations from the snowflake yeast could be applicable to the constraints posed on the intraspecific scaling exponent. But, it is possible that the selection paradigm used for the snowflake yeast could indirectly affect other genes directly responsible for metabolism. Further gene expression profiling is required to probe this possibility.

Some methods for characterizing the snowflake yeast, in the context of its growth rate dynamics, density variation and mass measurements have been described. The methods are promising, but the characterization is not complete yet. Of the 8 populations, only 5 have been characterized. These characterizations are essential for population level measurements of metabolic activity from the culture, like volume of CO_2 released, or microcalorimetry for total heat generated. If metabolic activity is to be probed at the individual level, the distributions of sizes in a given culture won't make a difference. In the next chapter, one such possible method for individual level metabolic activity is described.

References

1. Bonner, J. T. The origins of multicellularity. *Integrative Biology: Issues, News, and Reviews: Published in Association with The Society for Integrative and Comparative Biology* **1**, 27–36 (1998).
2. Does, A. & Bisson, L. F. Comparison of glucose uptake kinetics in different yeasts. *Journal of bacteriology* **171**, 1303–1308 (1989).
3. Don, M. The Coulter principle: foundation of an industry. *JALA: Journal of the Association for Laboratory Automation* **8**, 72–81 (2003).
4. Duina, A., A, M., Keeney, M. E. & B, J. Budding yeast for budding geneticists: a primer on the *Saccharomyces cerevisiae* model system. eng. *Genetics* **197**, 33–48. ISSN: 1943-2631 (Electronic); 0016-6731 (Print); 0016-6731 (Linking) (May 2014).
5. Errington, R. J. & White, N. S. in *Confocal microscopy methods and protocols* 315–340 (Springer, 1999).
6. Glazier, D. Metabolic Scaling in Complex Living Systems. *Systems* **2**, 451–540. ISSN: 2079-8954 (2014).
7. Godfrey-Smith, P. *Darwinian populations and transitions in individuality* (na, 2011).
8. Grover, W. H. *et al.* Measuring single-cell density. *Proceedings of the National Academy of Sciences* **108**, 10992–10996 (2011).
9. Herron, M. D., Rashidi, A., Shelton, D. E. & Driscoll, W. W. Cellular differentiation and individuality in the ‘minor’multicellular taxa. *Biological Reviews* **88**, 844–861 (2013).

10. Jacobeen, S., Graba, E. C., *et al.* Geometry, packing, and evolutionary paths to increased multicellular size. *Physical Review E* **97**. ISSN: 24700053. doi:10.1103/PhysRevE.97.050401. arXiv: 1802.03615 (May 2018).
11. Jacobeen, S., Pentz, J. T., *et al.* Cellular packing, mechanical stress and the evolution of multicellularity. *Nature Physics* **14**, 286–290. ISSN: 17452481 (Mar. 2018).
12. Łabędź, B., Wańczyk, A. & Rajfur, Z. Precise mass determination of single cell with cantilever-based microbiosensor system. *Plos one* **12**, e0188388 (2017).
13. Laurent, T. C., Pertof, H. & Nordli, O. Physical chemical characterization of percoll. i. particle weight of the colloid. *Journal of Colloid and Interface Science* **76**, 124–132 (1980).
14. Model, M. A. Methods for cell volume measurement. *Cytometry Part A* **93**, 281–296 (2018).
15. Oliver, R., Kinnear, A. & Ganf, G. Measurements of cell density of three freshwater phytoplankters by density gradient centrifugation 1. *Limnology and Oceanography* **26**, 285–294 (1981).
16. Pertof, H., Laurent, T., Seljelid, R., Kågedal, L., Hirtenstein, M., *et al.* in *Separation of Cells and Subcellular Elements* 67–72 (Elsevier, 1979).
17. Popescu, G., Park, K., Mir, M. & Bashir, R. New technologies for measuring single cell mass. *Lab on a Chip* **14**, 646–652 (2014).
18. Ratcliff, W. C., Denison, R. F., Borrello, M. & Travisano, M. Experimental evolution of multicellularity. *Proceedings of the National Academy of Sciences of the United States of America* **109**, 1595–1600. ISSN: 00278424 (Jan. 2012).
19. Ratcliff, W. C., Fankhauser, J. D., Rogers, D. W., Greig, D. & Travisano, M. Origins of multicellular evolvability in snowflake yeast. *Nature Communications* **6**. ISSN: 20411723. doi:10.1038/ncomms7102 (2015).
20. Ratcliff, W. C. & Travisano, M. *Experimental evolution of multicellular complexity in saccharomyces cerevisiae* 2014. doi:10.1093/biosci/biu045.
21. Rebolleda-Gómez, M., Ratcliff, W. C., Fankhauser, J. & Travisano, M. Evolution of simple multicellularity increases environmental complexity. doi:10.1101/067991. <<http://dx.doi.org/10.1101/067991>> (2016).
22. Schindelin, J. *et al.* Fiji: an open-source platform for biological-image analysis. *Nature methods* **9**, 676–682 (2012).
23. Thommen, A. *et al.* Body size-dependent energy storage causes Kleiber's law scaling of the metabolic rate in planarians. *eLife* **8**, 1–69. ISSN: 2050084X (2019).
24. Vembadi, A., Menachery, A. & Qasaimeh, M. A. Cell Cytometry: Review and Perspective on Biotechnological Advances. *Frontiers in Bioengineering and Biotechnology* **7**, 147. ISSN: 2296-4185 (2019).

Chapter 3

Measuring Metabolic Activity

There are innumerable measures for metabolic activity (*Lighton 2017; Butler et al. 2004; Speakman 2013; Tomlinson et al. 2018*). In addition to the quest for understanding fundamental aspects of metabolism, such measurement methods are extremely important in biomedicine. Subtle mismatches in metabolic activity, be it in energy acquisition, storage or utilization, are the root of many pathologies (*Lighton 2017*). Measurements of metabolic rate include oxygen uptake (*AU - Dietz et al. 2019*), carbon dioxide release (*Yatsenko et al. 2014*), heart rate (*Green 2011*), and heat release (*Burger & van Breukelen 2013*).

Flow through respirometers are chambers for measuring metabolic activity where the flow rate of air is maintained. If an organism is placed in such a chamber, the differences in gaseous concentrations in the incurrent and excurrent from the chamber would provide an estimate of oxygen consumption and carbon dioxide release. This method is limited by the sensitivity of the O_2 and CO_2 sensors, and the duration for which the organism is kept in the chamber for an accurate measurement (*Lighton 2017*). A more recent, more accurate measure of respirometry uses doubly labeled water, using stable isotopes of hydrogen and oxygen to trace the flow of water and CO_2 over time. This method can be used across all scales for measuring field metabolic rates (*Butler et al. 2004*). Isotope labeling has also been used for carbon and nitrogen uptake rates from phytoplankton (*Zaoli et al. 2019*). For animals, the heart rate is another measure for metabolic activity. The heart rate, if measured accurately, can provide good measures of maximal metabolic rates, basal metabolic rates, and field metabolic rates (*Green 2011*). Another popular method for measuring metabolic activity is calorimetry. Calorimetry measures the net heat production of an organism (*Hackney 2016*). Methods of measuring metabolic activity from cells include characterizing expression of genes relevant to metabolism (*Cubuk et al. 2019*), ATP assays (*Mendelsohn et al. 2018*), fluorescent tagging of enzymes (*Nozeret et al. 2019*), and from Clark electrodes for measuring oxygen consumption (*Li & Graham 2012*).

ATP assays and Clark electrodes can only be used for bulk measurements from a large number of cells, and not single cells. Given the variation among a population of cells, methods allowing for measuring metabolic activity from single cells are much more powerful tools than bulk measurement tools, as it aids in capturing the heterogeneity (*Hong et al. 2020*). In June 2020, Hong et al. described a non invasive and label free method to accurately perform nano-calorimetry in a microfluidic setup to

measure heat production from single cells of the algae, *Tetrahymena thermophile* (Hong et al. 2020). Other microfluidic tools for measuring metabolic activity from single cells have also been described (Boitard et al. 2012). In this report, I build on one such described microfluidic method.

3.1 Single Cell Metabolic Activity - A Microfluidic Method

A microfluidic method for measuring bioenergetics from single cells was described by Boitard et al in 2012. Their method involved trapping cells in aqueous droplets containing glucose, in a continuous phase of mineral oil and perfluorohexyloctane. The droplet containing cells are in contact with empty aqueous droplets (no cell) with the same concentration of glucose. As the cells metabolize glucose, the concentration of glucose in the droplet would reduce, generating an chemical potential across the droplet contacts. Driven by this chemical potential, water would flow out of the cell droplet into the empty droplets, causing it to shrink. By observing the dynamics of this shrinking, the rate of glucose consumption from a single cell can be estimated (Boitard et al. 2012). Woronoff et al. 2019 used the same method to measure the metabolic cost of adaptation in yeast cells (Woronoff et al. 2020).

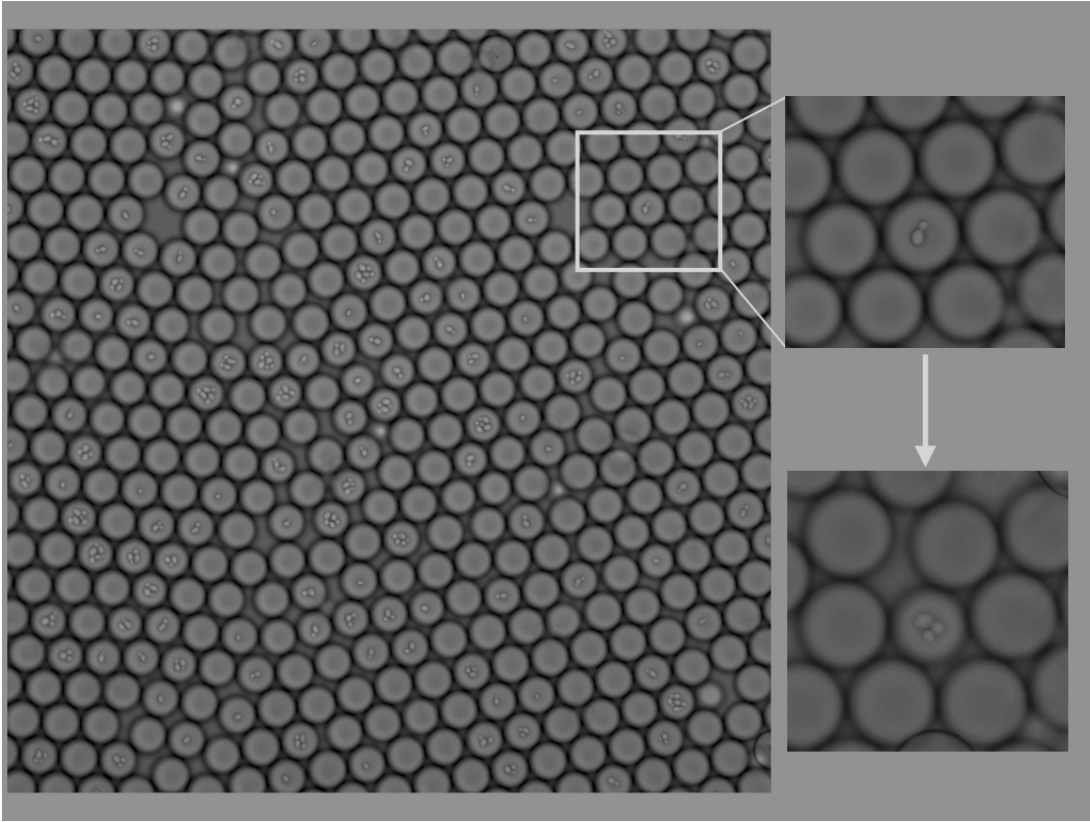


Figure 3.1: A grid of aqueous droplets with YPD and cells. Over time, as cells start to consume metabolites, the metabolite concentrations fall. In response to the change in concentration gradient, water flows out of the droplet with the cell. The inset shows an example of such a droplet

The principle here is that water droplets in oil can be stabilized by surfactants (Goodarzi & Zende-hboudi 2019). Using appropriate microfluidic devices and formulations of surfactants, different sizes of

stable droplets can be obtained. When these droplets come in contact, the surfactants form a bilayer membrane between the droplets (*Bayley et al. 2008*). A concentration mismatch can drive movement of solute or solvent across the membrane (*Comper & Williams 1992*).

In an attempt to replicate the method used in by Boitard et al. 2012, a flow focusing device was used to make mono-disperse droplets with a radius of nearly $50\mu\text{m}$. An appropriate dilution of a yeast cell culture in YPD was chosen such that some droplets contain single cells. While using the setup described in Boitard et al. 2012, I discovered some inconsistencies in the method and analysis. Firstly, the dynamics of shrinkage depends on the number of contacts a droplet has. Over time, as the droplet shrinks, the number of contacts can change. In Figure 1, a droplet starting out with 6 contacts has 4 after 10 hours. Given an image time series, it is difficult to point out, with certainty if the number of contacts have changed from frame to frame (Figure 3.1).

The analysis protocol used in the paper make some assumptions that are not necessarily true in experiment. The authors assume that the concentration of glucose in the empty droplets remains the same. For this assumption to hold true, the number of droplets with cells need to be far lower than the number empty droplets. Doing so would reduce the throughput of the method drastically. Secondly, it is assumed that the area of contact between two droplets remains the same as the droplet shrinks. Ideally, the area of contact would depend on the radius of the droplet. The radius dependence on the area would be important for the dynamics of radius change.

I propose here, a new possible method, using the same principles of osmotic ripening which is free of the aforementioned inconsistencies.

3.2 A Droplet-in-Droplet Method

To avoid the difficulties in the previous method, a setup is required where the number of contacts does not change, where the concentration difference across the membranes is known throughout, while allowing high throughput. The easiest setup for having control over the concentrations is to have the droplets with cells in contact with an infinite reservoir. The droplets with cells should not be in contact with droplets containing cells. This way, each droplet has only one contact.

To implement this, I set-up a system as described in Figure 3.2. An aqueous droplet is trapped in a larger droplet of fluorinated oil. This droplet in droplet system is then immersed into an aqueous bath. Fluorinated oils are denser than water. We exploit this difference in density in our setup. The oil droplet sinks to the bottom of the bath. The aqueous droplet floats to the top of the oil droplet. The surfactants form a bilayer at the interface between the aqueous droplet and the bath. A cell can be trapped in the inner aqueous droplet. In this setup, the aqueous droplets do not touch each other, and any observed radius change won't be affected by other droplets.

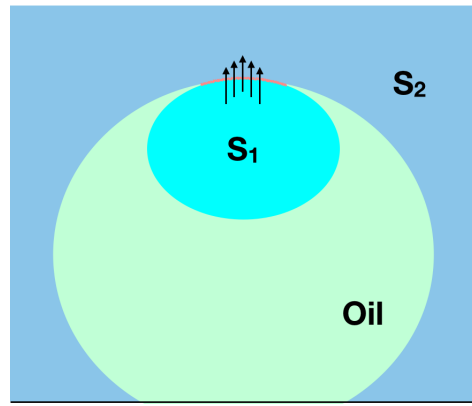


Figure 3.2: Schematic of droplet set-up used. An aqueous droplet with a concentration of solutes (S_1) is trapped in a droplet of fluorinated oil. The droplet in droplet system is placed in an aqueous bath, with solute concentration S_2 . If $S_1 < S_2$, water can flow out of the droplet in response to the osmotic gradient

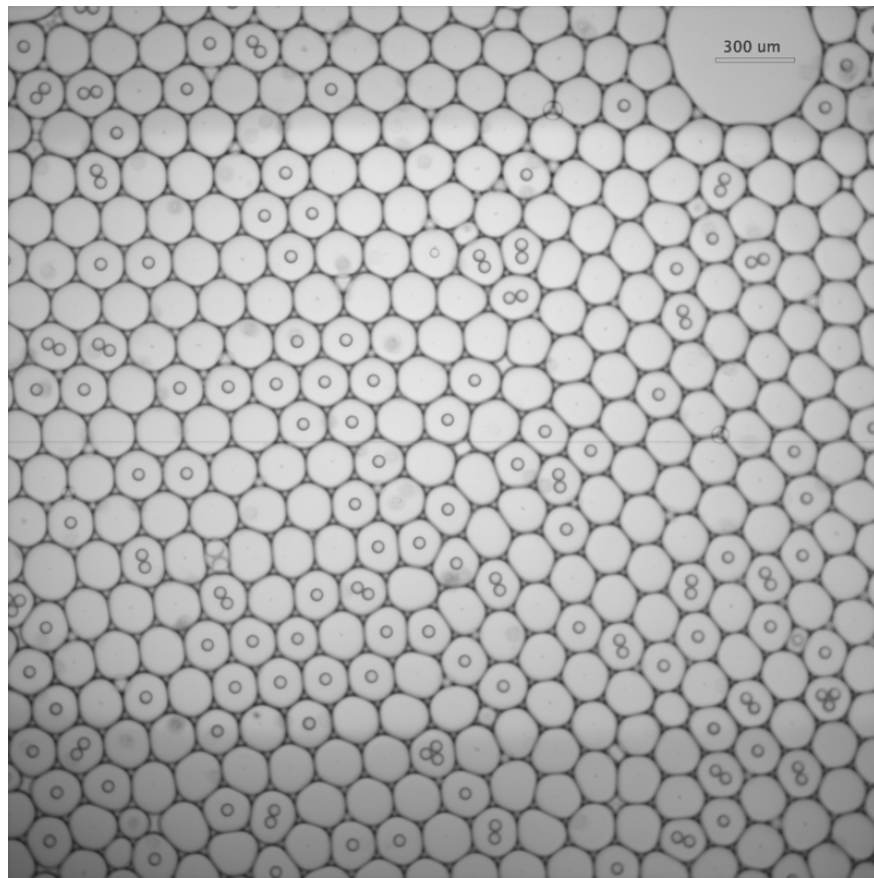


Figure 3.3: Image of droplet-in-droplet setup. In the ideal scenario, all the packed oil droplets would have a single aqueous droplet. The aqueous droplets are in contact with the outer aqueous bath

The fluorinated oil HFE7500 (3M HFE 7500 NOVEC Engineered Fluid) was used for the setup. Aqueous droplets were stabilized in this fluorinated oil continuous phase using 2.5% Pico-Surf, a biocompatible surfactant (*Yan et al. 2013*). The larger oil droplets were stabilized in the aqueous continuous phase with 0.2% SDS. Details on the microfluidic devices that were used to make this setup, and the continuous phase used are provided as an Appendix.

Given a concentration difference of ΔC across a membrane of cross sectional area A , the volume transferred across the membrane would have the following time dependence (*Fick 1855*):

$$\frac{dV(R)}{dt} = p_k \Delta C A \quad (3.1)$$

where p_k is the permeability coefficient. In our setup, ΔC changes with time, and is dependent on the radius of the droplet.

$$\Delta C = C_{in}(R) - C_{out} \quad C_{in}(R) = \frac{3N}{4\pi R^3}$$

where N is the time independent number of solute molecules in the droplet. The assumption here is that any chemical imbalance drives the movement of water, and not glucose or other solutes. The area of contact can be represented as $A = K_{ow}R^2$, where K_{ow} depends on the oil, aqueous phase and the oil used (*Bayley et al. 2008*). For this analysis, this is assumed to be a constant. Assuming the droplet to be a sphere, the above equation can be written as:

$$4\pi R^2 \frac{dR}{dt} = p_k \left(\frac{3N}{4\pi R^3} - C_{out} \right) K_{ow} R^2$$

$$\frac{dR}{dt} = \frac{p_k K_{ow}}{4\pi} \left(\frac{3N}{4\pi R^3} - C_{out} \right) \quad (3.2)$$

To corroborate this model, controls were done with different solutions in the aqueous droplet and in the bath. It is also essential to estimate the constant in equation 3.2 if the rates of glucose consumption from cells is to be estimated by the dynamics of droplet shrinkage. From the timeseries of microscope images of the droplet-in-droplet system, the aqueous droplets were identified using a Circular Hough transform. Circles were plotted over the image to identify appropriately identified droplets.

Firstly, it is important to confirm that the droplet size does not change when there is no concentration gradient. For this, aqueous droplets containing YPD media (yeast growth media) were used, in a bath containing the same YPD media.

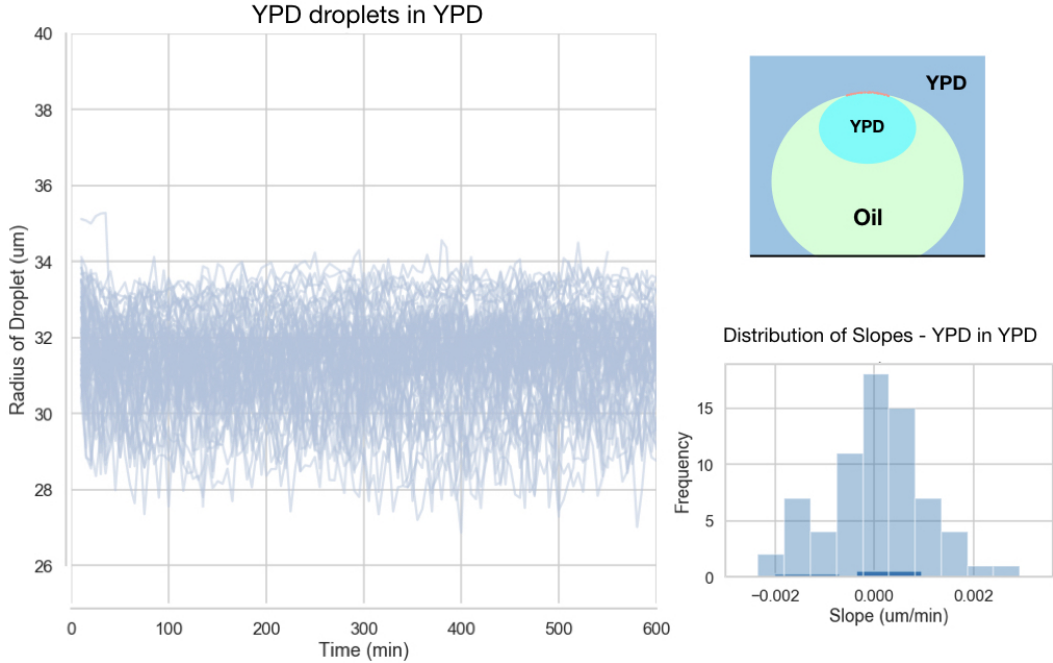


Figure 3.4: With no concentration gradient, the droplet sizes do not change with time. The setup had 20g/L glucose solution in the aqueous droplet and the bath.

The concentration gradient is 0. A linear fit on the 70 droplets analyzed (Figure x) shows that there is indeed no change in the droplet size over 10 hours.

With glucose, yeast metabolism is dominated by fermentation (*Feldman 2012*): $C_6H_{12}O_6 \rightarrow 2C_2H_5OH + 2CO_2$. If a cell is to perform this reaction in the droplet, the byproducts, ethanol and carbon dioxide should not affect droplet shrinkage. CO_2 is highly soluble in hydrofluoroethers (HFE) (*Mamone et al. 2015*). To confirm that ethanol does not affect droplet shrinkage, aqueous droplets of 20g/L glucose and 1M ethanol were observed when immersed in a bath of 20g/L glucose.

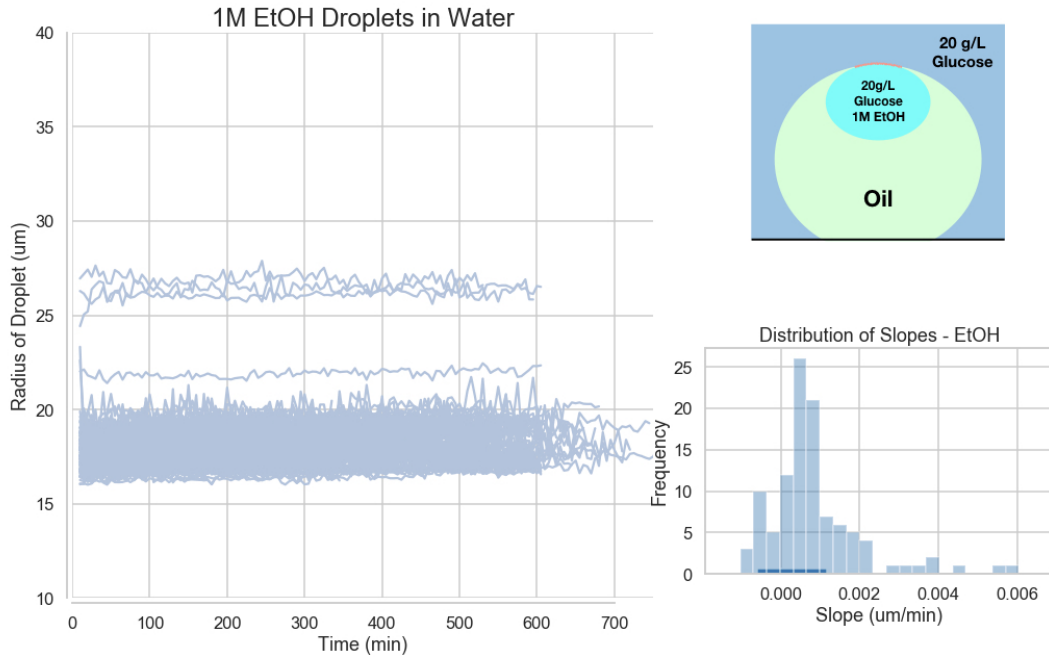


Figure 3.5: With 1M EtOH in the aqueous droplet, there is no shrinkage. The setup had 1M EtOH in 20g/L glucose solution in the aqueous droplet and 20g/L glucose solution in the bath. 107 droplets were analysed for this control

This indicates that an ethanol concentration mismatch does not affect the change in droplet radius. There are 2 possibilities for this. One, that ethanol diffused across the membrane instead of water in response to its concentration gradient. 1M Ethanol is 5% EtOH, 95% Water. The volume contribution of Ethanol diffusing across the membrane to the change in droplet size is negligible. The other possibility is that Ethanol has some non-zero solubility in the fluorinated oil, and diffused into the oil. Either way, this control confirms that an ethanol concentration mismatch does not contribute to changes in the droplet radius.

From Equation 2, the easiest way to estimate the constant term is to have $N = 0$, such that:

$$\frac{dR}{dt} = \frac{p_k K_{ow}}{4\pi} C_{out}$$

The rate of change in radius should be constant. An aqueous droplet with no solutes, when in a bath with 20g/L glucose shrinks in accordance with this differential equation (Figure 3.6)

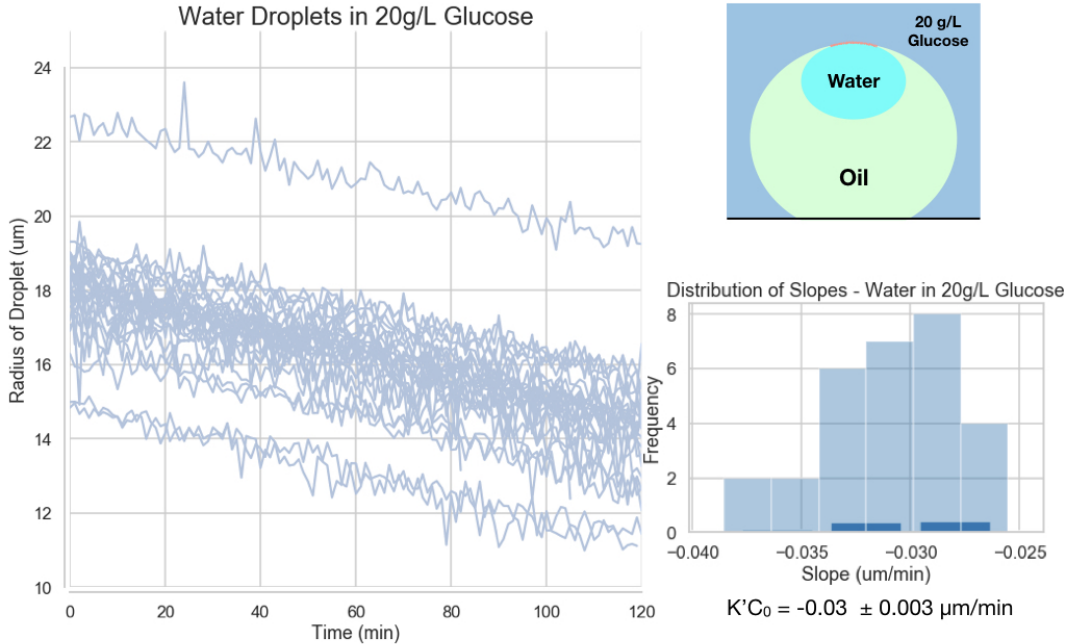


Figure 3.6: The droplet radius shrinkage is linear with time when there are no solute molecules in the aqueous droplet. In this setup, the inner droplet has water, and the outer bath is a 20g/L glucose solution. 29 droplets were analysed.

The slope here is $0.03 \pm 0.003 \mu\text{m}/\text{min}$.

Yeast cells are to grow in droplets containing the yeast growth media YPD. To extract information about metabolic rate from the droplets, the constant term in Equation 2 must be calculated for YPD. Droplets of water, with no solutes were observed when in a bath of YPD to estimate the constant term.

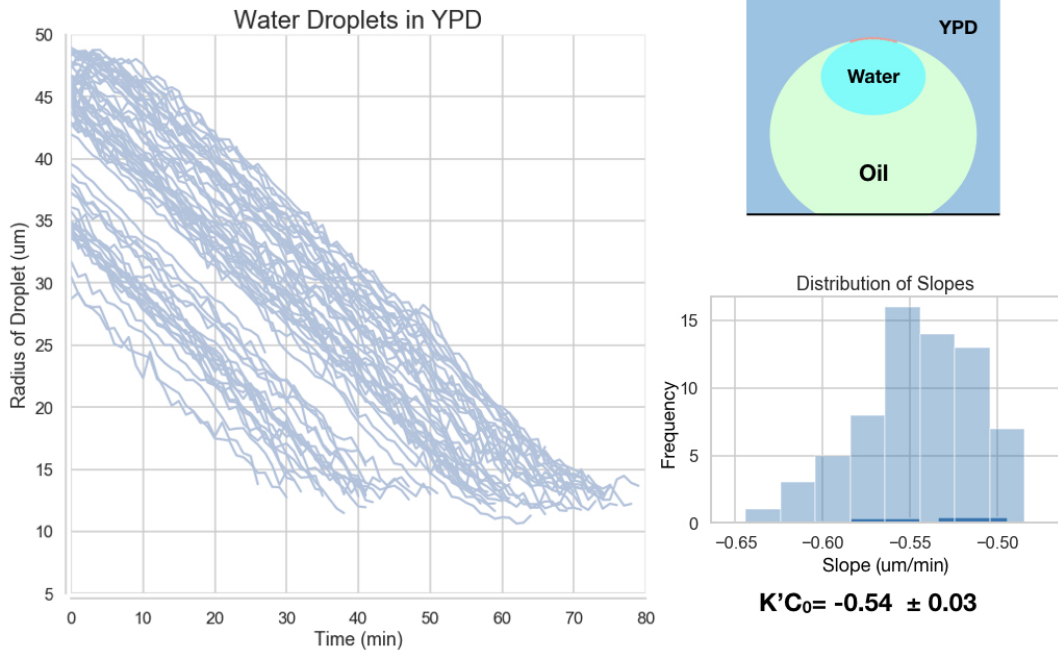


Figure 3.7: The droplet radius shrinkage is linear with time when there are no solute molecules in the aqueous droplet. In this setup, the inner droplet has water, and the outer bath has YPD

Note that YPD has multiple chemical constituents in it. It is made of yeast extract, tryptone and glucose (*Treco & Lundblad 1993*). The estimated constant $p_k K_{ow} C_{out} / 4\pi$ is actually $(K_{ow}/4\pi) \sum_i p_k^{(i)} C_{out}^{(i)}$, summed over all the constituent components.

For YPD, the constant is estimated at $0.54 \pm 0.03 \mu\text{m}/\text{min}$. Given the number of constituents, it is expected that the constant be greater than what is measured for water in Figure 3.6.

To confirm that equation 2 captures the dynamics of the system properly, it is also essential to observe shrinkage of droplets with non zero concentrations of solutes in it.

Due to experimental constraints, the observation of droplets starts only after 8-12 minutes after they come in contact with the bath. For this reason, the initial radius of the droplet could not be accurately measured. But, the final radius of the droplet can be measured and used to estimate the number of solute particles in the droplet. From equation 2, the droplet size is expected to stop changing when $C_{in} = C_{out}$, i.e. when $\frac{3N}{4\pi R_\infty^3} = C_{out}$. The above equation, in terms of R_∞ is:

$$\frac{dR}{dt} = \frac{p_k K_{ow} C_{out}}{4\pi} \left[\left(\frac{R_\infty}{R} \right)^3 - 1 \right] \quad (3.3)$$

YPD media is diluted to twice its volume with water and trapped as an aqueous droplet. The shrinkage of the droplet when placed in a bath of YPD is observed. The data was fit to the differential equation 3 to estimate the constant $p_k K_{ow} C_{out}/4\pi$, using the SciPy Python package (*Virtanen et al. 2020*).

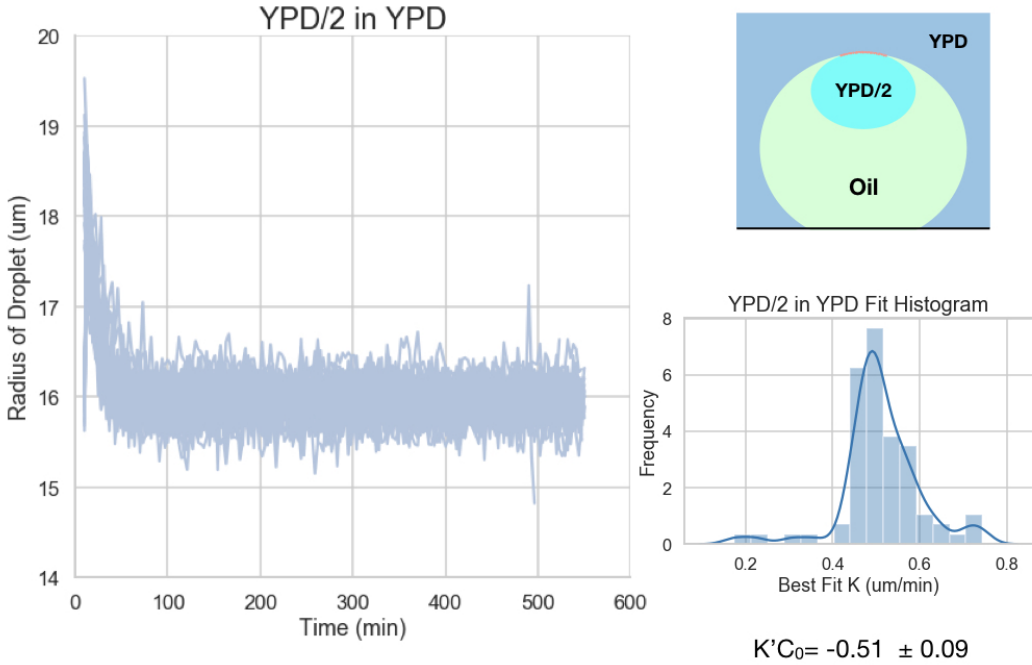


Figure 3.8: With YPD diluted to twice its volume in the droplet, and YPD in the bath, the droplet shrinkage is as given. The droplet stops shrinking when the concentrations inside the droplet matches with the bath. The inset histogram shows the distribution of fits for the constant in Equation 3. 87 droplets were analysed.

The equation fits the obtained experimental data well. Some examples of the fit are given in Figure 3.8. The estimated constant here is $-0.51 \pm 0.09 \mu\text{m}/\text{min}$, which is also in accordance with the constant obtained using water droplets in YPD, as in Figure 3.6.

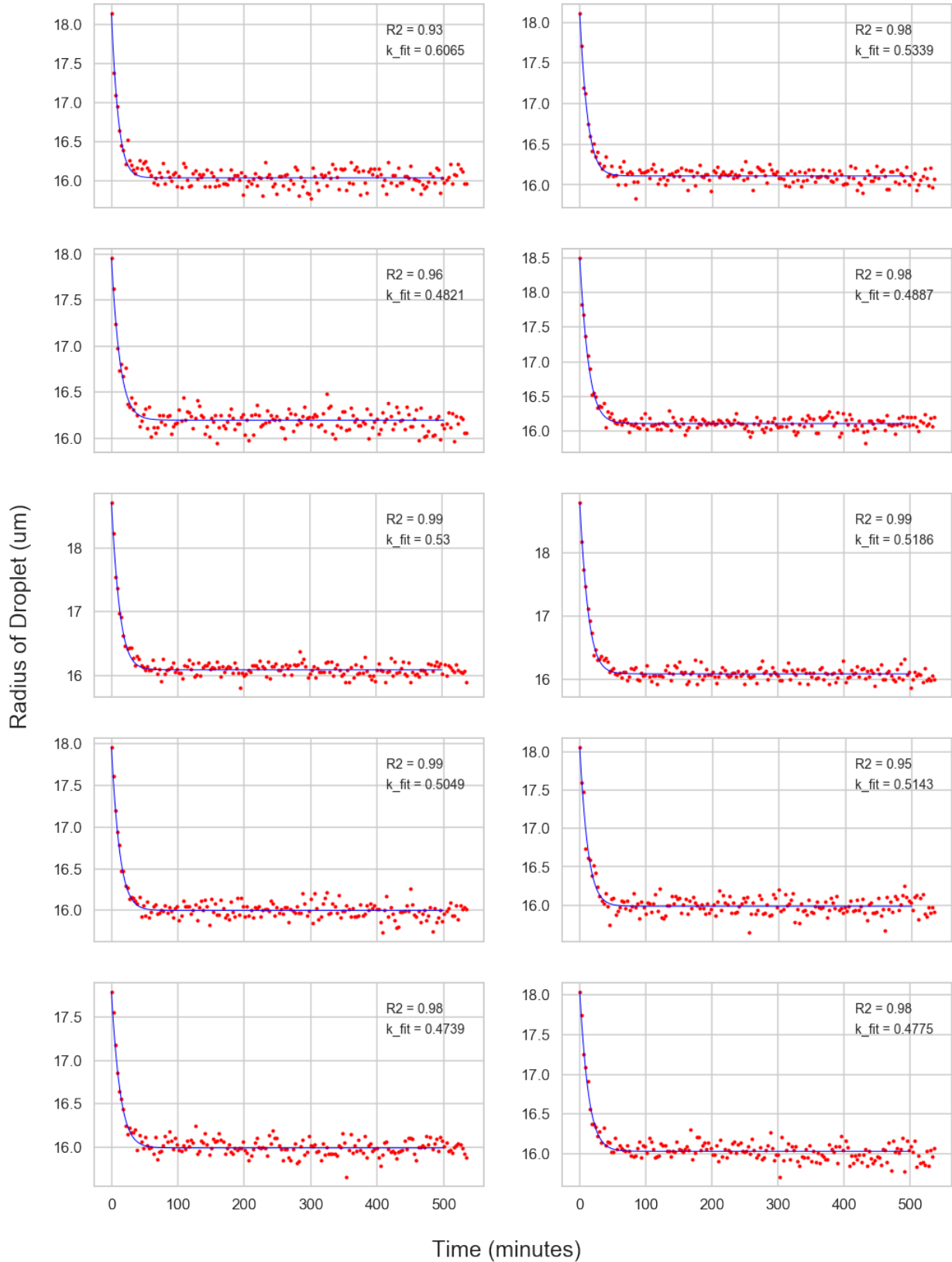


Figure 3.9: Some examples of fits of Equation 3 (blue) to droplet shrinkage dynamics (red) for droplets with YPD diluted to four times, in a bath of YPD. R^2 is estimated using the first 20 points of the dataset

In another setup, YPD diluted to four times its volume with water was trapped in a droplet and its shrinkage was observed when placed in a bath of YPD.

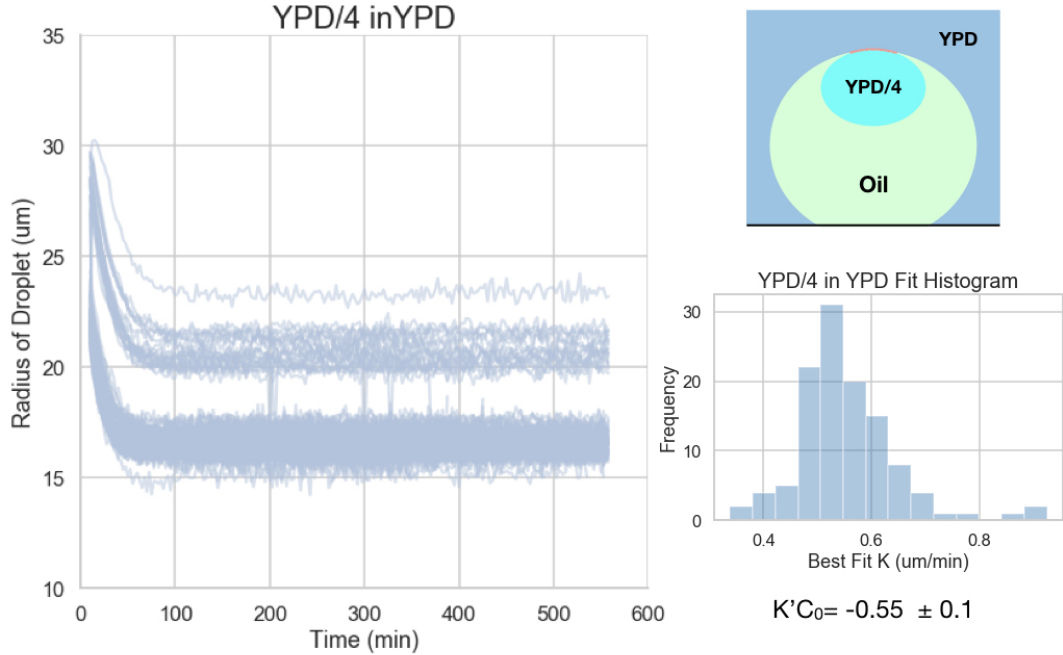


Figure 3.10: With YPD diluted to four times its volume in the droplet, and YPD in the bath, the droplet shrinkage is as given. The droplet stops shrinking when the concentrations inside the droplet matches with the bath. The inset histogram shows the distribution of fits for the constant in Equation 3.

In this particular setup, the initially obtained aqueous droplets were poly-disperse, i.e. were of varying sizes. This results in different droplets having different shrinking trajectories. Nonetheless, the differential equation model captures the dynamics of shrinkage for all the droplets well. Some examples of the fit are given in Figure 3.9. The estimated constant is very similar to those estimated in other controls (Figure 3.8, Figure 3.6).

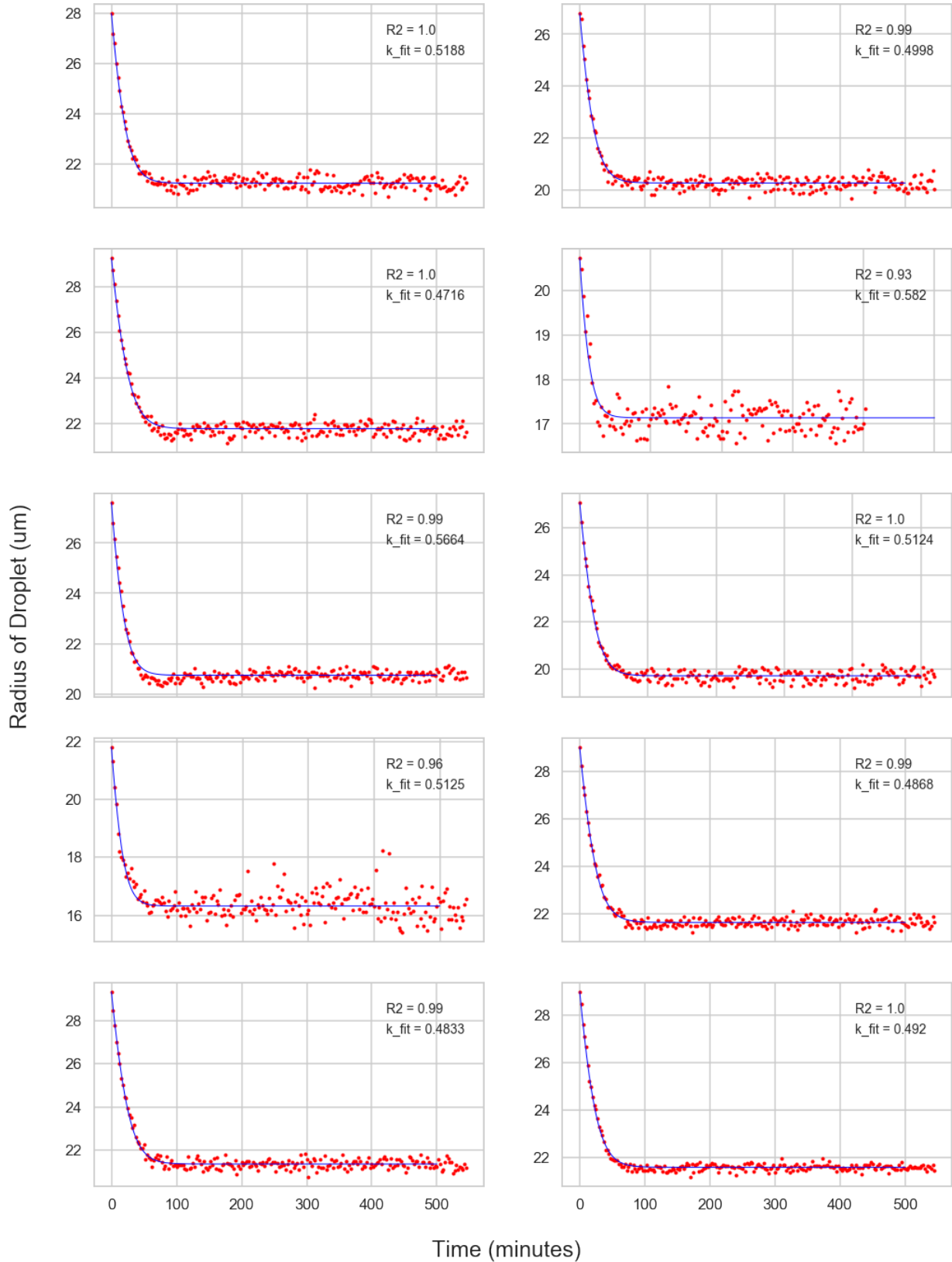


Figure 3.11: Some examples of fits of Equation 3 (blue) to droplet shrinkage dynamics (red) for droplets with YPD diluted to four times, in a bath of YPD. R^2 is estimated using the first 20 points of the dataset

If a cell is put into the droplet, assuming a constant rate of metabolic uptake β , $N = N_0 - n\beta t$, where n is the number of cells in the droplet. Using this in Equation 3.2,

$$\frac{dR}{dt} = \frac{p_k K_{ow}}{4\pi} \left(\frac{3(N_0 - n\beta t)}{4\pi R^3} - C_{out} \right) \quad (3.4)$$

$N_0 = \frac{4\pi R_0^3}{3}$ can be used to estimate β using the above equation. The number of cells n can be obtained by inspecting the time series images of the droplets.

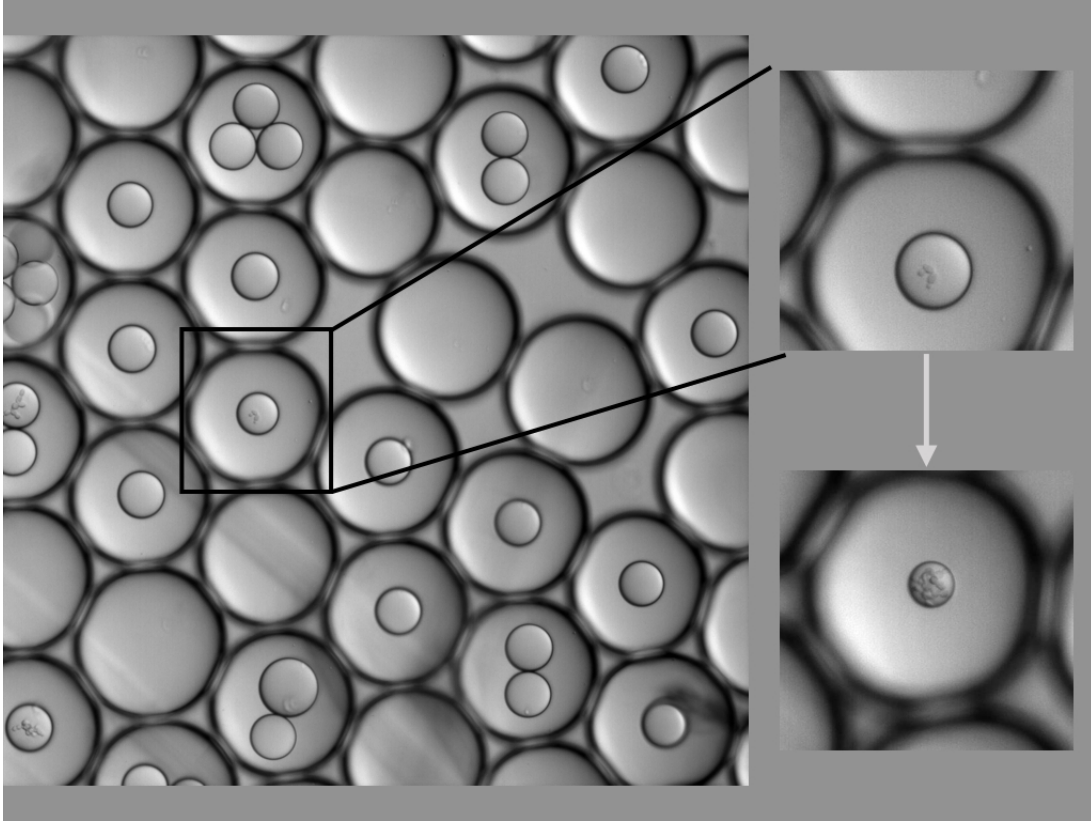


Figure 3.12: The Droplet in Droplet system with cells. Ideally, each oil droplet has one aqueous droplet, and each aqueous droplet starts with a single cell. Over time the cell consumes glucose, and the droplet shrinks

I was able to trap 2 viable cells in droplets with YPD and observe shrinkage when put in a bath of YPD (Figure 3.13). Unfortunately, due to experimental errors, metabolic activity cannot be estimated from this data. The yeast cells were in the droplet for over an hour before imaging started. As a result, the initial concentration of YPD when imaging starts is not known. Without this information, the differential equation cannot be fit to collected data. On a positive note, the droplet shrinking trajectories for these cells are similar (Figure 3.13)

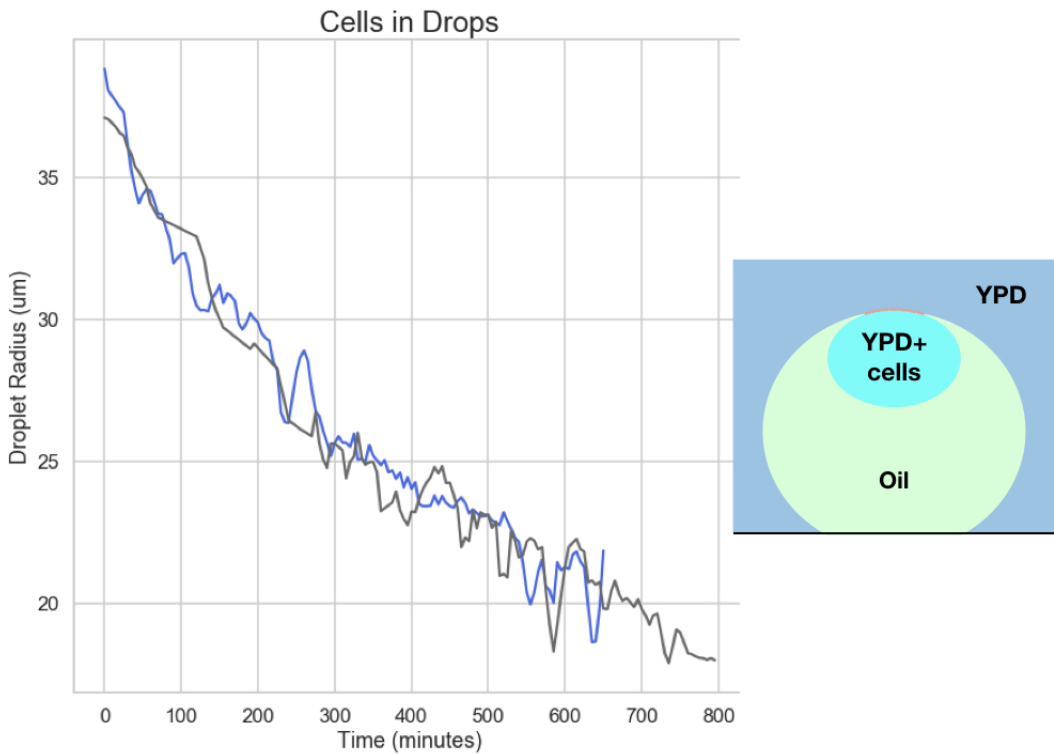


Figure 3.13: Droplet Shrinkage for the droplets containing cells (Gray and Blue plots correspond to one droplet each). They seem to follow the same trajectories.

3.3 Caveats

Inverse emulsion droplets (water in oil) have been very useful in microfluidic biological applications, for individual assays, amplification, or compartmentalizing biomolecules or cells (*Rakiszewska et al. 2014; Kaminski et al. 2016*). The set-up presented here is a promising method for measuring metabolic activity from single cells. Metabolic by-products do not affect droplet shrinkage. The equations proposed explain the dynamics of droplet shrinkage in the controls conducted. Further characterization is required to estimate constants that are important for the dynamics of droplet shrinkage. This method could also have potential biomedical applications. By changing the contents of the aqueous droplet, metabolic activity from pathologically relevant cells can be measured. Modifications would need to be made if these cells need a physical substrate to grow on.

But, when considering this droplet in droplet method, there are some caveats:

- It is assumed that the consumption of media is stoichiometric, i.e. at all given times, the ratio of components in the growth medium is constant. This is not necessarily true, as cellular uptake rates for different components of growth media could be different.

- Metabolic activity could very well be dependent on feedback from neighboring cells. In bacteria, quorum sensing restricts glucose uptake and reduces metabolic rate when crowded (*An et al. 2014; Davenport et al. 2015*). So, the metabolic rate measured from single cells may not be the metabolic rates cells exhibit in non-experimental conditions; conditions which have shaped the evolutionary history of the cells.
- The aqueous droplet has to be much larger than the cell. At the limit where the cell size is similar to the droplet size, flow of metabolites could be affected, and therefore uptake.
- The cells continue to grow in the droplet. The measured metabolic rate is therefore contributed by all these cells. These can be counted, but the assumption is that being derived from a single, there is homogeneity in metabolic activity.
- It is possible that cells are killed in the process of trapping in the aqueous droplet, at the microfluidic device. I attempted to measure from cells on 4 separate occasions, observing over 100 droplets with cells. Of these, only 2 droplets had viable cells that divided and consumed glucose. This problem can be circumvented by modifying the procedure at the droplet making step to reduce any possible physical stress on the cells.

Nonetheless, the proposed method is extremely promising for measuring metabolic activity from the yeast snowflake. By modifying the microfluidic devices used to generate the droplets, larger droplets, which can accommodate the yeast snowflake can be made. Given the longer generation time for the snowflake , the fourth caveat can be dismissed.

References

1. An, J. H., Goo, E., Kim, H., Seo, Y.-S. & Hwang, I. Bacterial quorum sensing and metabolic slowing in a cooperative population. *Proceedings of the National Academy of Sciences* **111**, 14912–14917. ISSN: 0027-8424 (2014).
2. AU - Dietz, L. J. *et al.* Measuring and Interpreting Oxygen Consumption Rates in Whole Fly Head Segments. *JoVE*, e58601 (2019).
3. Bayley, H. *et al.* Droplet interface bilayers. eng. *Mol Biosyst* **4**, 1191–1208. ISSN: 1742-2051 (Electronic); 1742-206X (Print); 1742-2051 (Linking) (Dec. 2008).
4. Boitard, L. *et al.* Monitoring single-cell bioenergetics via the coarsening of emulsion droplets. *Proceedings of the National Academy of Sciences* **109**, 7181–7186 (2012).
5. Burger, M. & van Breukelen, F. Construction of a low cost and highly sensitive direct heat calorimeter suitable for estimating metabolic rate in small animals. *Journal of Thermal Biology* **38**, 508–512 (2013).
6. Butler, P. J., Green, J. A., Boyd, I. & Speakman, J. Measuring metabolic rate in the field: the pros and cons of the doubly labelled water and heart rate methods. *Functional ecology* **18**, 168–183 (2004).
7. Comper, W. D. & Williams, R. P. W. *Mechanism of Osmotic Flow in Mechanics of Swelling* (ed Karalis, T. K.) (Springer Berlin Heidelberg, Berlin, Heidelberg, 1992), 743–761. ISBN: 978-3-642-84619-9.

8. Çubuk, C. *et al.* Differential metabolic activity and discovery of therapeutic targets using summarized metabolic pathway models. *npj Systems Biology and Applications* **5**, 7 (2019).
9. Davenport, P. W., Griffin, J. L. & Welch, M. Quorum Sensing Is Accompanied by Global Metabolic Changes in the Opportunistic Human Pathogen *Pseudomonas aeruginosa*. *Journal of Bacteriology* **197** (ed O'Toole, G. A.) 2072–2082. ISSN: 0021-9193 (2015).
10. Feldman, H. in *Yeast* 25–58 (John Wiley and Sons, Ltd, 2012). ISBN: 9783527659180. doi:10.1002/9783527659180.ch3. eprint: <https://onlinelibrary.wiley.com/doi/pdf/10.1002/9783527659180.ch3>. <<https://onlinelibrary.wiley.com/doi/abs/10.1002/9783527659180.ch3>>.
11. Fick, D. A. V. On liquid diffusion. *The London, Edinburgh, and Dublin Philosophical Magazine and Journal of Science* **10**, 30–39 (1855).
12. Goodarzi, F. & Zendehboudi, S. A Comprehensive Review on Emulsions and Emulsion Stability in Chemical and Energy Industries. *The Canadian Journal of Chemical Engineering* **97**, 281–309 (2019).
13. Green, J. A. The heart rate method for estimating metabolic rate: Review and recommendations. *Comparative Biochemistry and Physiology Part A: Molecular And Integrative Physiology* **158**. The challenge of measuring energy expenditure: current field and laboratory methods, 287–304. ISSN: 1095-6433 (2011).
14. Hackney, A. C. in *Exercise, Sport, and Bioanalytical Chemistry* (ed Hackney, A. C.) 33–42 (Elsevier, 2016). ISBN: 978-0-12-809206-4. doi:<https://doi.org/10.1016/B978-0-12-809206-4.00013-5>. <<http://www.sciencedirect.com/science/article/pii/B9780128092064000135>>.
15. Hong, S. *et al.* Sub-nanowatt microfluidic single-cell calorimetry. *Nature Communications* **11**, 2982 (2020).
16. Kaminski, T. S., Scheler, O. & Garstecki, P. Droplet microfluidics for microbiology: techniques, applications and challenges. *Lab on a Chip* **16**, 2168–2187 (2016).
17. Li, Z. & Graham, B. H. in *Mitochondrial Disorders* 63–72 (Springer, 2012).
18. Lighton, J. R. B. Limitations and requirements for measuring metabolic rates: a mini review. *European Journal of Clinical Nutrition* **71**, 301–305 (2017).
19. Mamone, M., Milcent, T. & Crousse, B. Reactivity of carbon dioxide in hydrofluoroethers: a facile access to cyclic carbonates. *Chemical Communications* **51**, 12736–12739 (2015).
20. Mendelsohn, B. A. *et al.* A high-throughput screen of real-time ATP levels in individual cells reveals mechanisms of energy failure. *PLoS biology* **16**, e2004624–e2004624 (Aug. 2018).
21. Nozeret, K., Boucharat, A., Agou, F. & Buddelmeijer, N. A sensitive fluorescence-based assay to monitor enzymatic activity of the essential integral membrane protein Apolipoprotein N-acyltransferase (Lnt). *Scientific Reports* **9**, 15978 (2019).
22. Rakowska, A., Tel, J., Chokkalingam, V. & Huck, W. T. One drop at a time: toward droplet microfluidics as a versatile tool for single-cell analysis. *NPG Asia Materials* **6**, e133–e133 (2014).
23. Speakman, J. R. Measuring energy metabolism in the mouse - theoretical, practical, and analytical considerations. *Frontiers in physiology* **4**, 34–34 (Mar. 2013).
24. Tomlinson, S. *et al.* Measuring metabolic rates of small terrestrial organisms by fluorescence-based closed-system respirometry. *Journal of Experimental Biology* **221**. ISSN: 0022-0949. doi:10.1242/jeb.172874. eprint: <https://jeb.biologists.org/content/221/7/jeb172874.full.pdf>. <<https://jeb.biologists.org/content/221/7/jeb172874>> (2018).

25. Treco, D. A. & Lundblad, V. Preparation of yeast media. *Current protocols in molecular biology* **23**, 13–1 (1993).
26. Virtanen, P. *et al.* SciPy 1.0: fundamental algorithms for scientific computing in Python. *Nature methods* **17**, 261–272 (2020).
27. Woronoff, G. *et al.* Metabolic cost of rapid adaptation of single yeast cells. *Proceedings of the National Academy of Sciences* **117**, 10660–10666. ISSN: 0027-8424 (2020).
28. Yan, J. *et al.* Monodisperse Water-in-Oil-in-Water (W/O/W) Double Emulsion Droplets as Uniform Compartments for High-Throughput Analysis via Flow Cytometry. *Micromachines* **4**, 402–413. ISSN: 2072-666X (2013).
29. Yatsenko, A. S., Marrone, A. K., Kucherenko, M. M. & Shcherbata, H. R. Measurement of metabolic rate in *Drosophila* using respirometry. *Journal of visualized experiments : JoVE*, e51681–e51681 (June 2014).
30. Zaoli, S. *et al.* Generalized size scaling of metabolic rates based on single-cell measurements with freshwater phytoplankton. *Proceedings of the National Academy of Sciences* **116**, 17323–17329. ISSN: 0027-8424 (2019).

Chapter 4

Discussion

4.1 The Yeast Snowflake - An experimental model for allometry

Experimental model systems are a necessity in the endeavor for understanding metabolic scaling. The snowflake yeast (*Ratcliff et al. 2012*), an experimentally evolved *Saccharomyces cerevisiae* system provides significantly greater advantages, in terms of variation in size, and experimental manipulability than previously described experimental systems for metabolic scaling, like modular organisms (*Burgess et al. 2017*) or planaria (*Thommen et al. 2019*).

The genetic toolkit available in yeast allows for experimental manipulations (*Bainbridge 1987*) of surface areas, resource demand, resource transport networks, and system compositions; the major possible constraints for metabolic scaling (*Glazier 2018*). Although, in such genetic manipulations as proposed below, it is vital to consider the possibility of metabolic activity being affected by indirect mechanisms or yet uncharacterized side effects of the mutations.

In yeast, glucose is stored as glycogen and trehalose (*François & Parrou 2001*). The enzymes responsible for the storage and utilization is known. Other nutrient stores include fats. Al-Anzi et al. (2015) describe a protein network that controls fat storage in *S. cerevisiae* (*Al-Anzi et al. 2015*). Appropriate modifications in regulators of certain genes would change the baseline system composition of yeast.

If cell size is increased, the surface area to volume ratio would change. Control over the cell size would allow for control over the surface area. Dungrawala et al. 2012 identified a set of genes responsible for control of cell size. Deletion of *WHI5* results in smaller cells. Deletion of *CLN3*, *BCK2*, *SWI4* or *SWI6* causes a cell cycle delay and results in larger cells (*Dungrawala et al. 2012*).

Resource demand in cells is driven by signaling networks, primarily centered on Ras/protein kinase A, AMP- activated kinase, or target of rapamycin complex I. The structure and interaction of these signaling networks in yeast has been characterised (*Broach 2012*). Changing the regulation of appropriate genes would allow for control over resource demand from the yeast cell.

The mechanisms of resource transport in the yeast snowflake is not well characterized yet. Tracing movement of fluorescent beads added to the growth media would provide details of resource movement

at the preliminary level. Fluorescent glucose can also be used for tracking movement of resources from the uptake source, across the snowflake.

As an added advantage, the metabolic network of yeast is well characterised. The current version of the database, Yeast Genome-scale metabolic models 7.6 (Yeast GEM 7.6) describes 1147 genes responsible for 3989 reactions involving 2693 metabolites (*Lu et al. 2019*).

The filter based method for measuring mass described here is a jugaad and works, but it may not be the most reliable method. The state of the art for measuring mass and density is the suspended microchannel resonator (*Grover et al. 2011*). The challenges associated with using this for the snowflake yeast has been detailed in Chapter 3. Given enough time, an array of SMR setups can be calibrated and used for precise determination of single cluster mass. Coupling SMR with the droplet-in-droplet method for measuring metabolic activity, the snowflake system can provide a precise and accurate allometric scaling relationship.

Multiple bulk methods for measuring metabolic activity should also be used to corroborate and confirm the measured rates. Microcalorimetry is one such promising method (*Hong et al. 2020*). My colleagues at the Thutupalli Lab at NCBS are working towards making accurate measurements of metabolic activity from the yeast snowflake using microcalorimetry. Another approach involves time resolved fluorescent measurements of the snowflake, in the presence of fluorescent glucose (2-NBDG) in the media (*Yoshioka et al. 1996*).

Measurements of density from the snowflake yeast negate the commonly used constant density assumption of most hypotheses pertaining to allometric scaling. Although further characterization is required for understanding how density varies with size, the resulting relationships should also be incorporated into future theories attempting to explain the relationship between metabolic activity and mass.

4.2 The Droplet-in-Droplet method for measuring metabolic activity

A method for measuring metabolic activity from single cells/clusters has been proposed in this report. The method builds on previously published microfluidic tools for measuring bioenergetics from single cells (*Boitard et al. 2012*). Metabolic activity can be measured by the rates of shrinkage of droplets containing cells. The droplet-in-droplet system proposed here allows for better control over the factors affecting the dynamics of shrinking. As a result, the measured metabolic activity is expected to be more reliable than results from the previously described method.

The droplet-in-droplet system is a promising method. The dynamics of droplet shrinkage in controlled setups are well described by derived dynamical equations. Ethanol, a metabolic waste product from yeast does not affect the rates of shrinkage. Further controlled setups need to be monitored and analyzed to estimate the appropriate values of relevant constants.

The method described here can be used outside the scope of the snowflake too. With further characterization pertaining to the effects of metabolic waste products, the system can be used to estimate

metabolic activity from other cells too. The tool has potential biomedical applications, given that changes in metabolic rates are the ‘underlying root of many pathologies’ (*Lighton 2017*).

4.3 Implications from Allometric Scaling of Metabolic Activity

The apparent power law relationship between metabolic activity and body size, ranging over 21 orders of magnitude indicates a fundamental constraint on metabolism (*Makarieva et al. 2008*). Multitudes of hypotheses, considering different constraints and mechanisms have been posed to explain the apparent relationship. These have been reviewed in Chapter 1. The empirical evidence collected over a century has been subjected to multiple statistical analyses. The recent analyses agree that there is a relationship between metabolic rate and body mass, and that the exponent is most likely not 3/4, as explained in most hypotheses.

Metabolic scaling relationships allow for predicting biological processes at individual, population, community and ecosystem levels (*Zaoli, Giometto, Marañón, et al. 2019*). This is the driving principle being the metabolic theory of ecology. The scaling dependance has been used to predict the distribution of heights of trees in tropical forests (*Anfodillo et al. 2013*), covariation of macro-ecological scaling laws, and variation in species diversity across islands on the basis of land area (*Zaoli, Giometto, Giezendanner, et al. 2019*). The metabolic scaling relationship provides insights on resource utilization in ecosystems (*Glazier 2018; Brown 2004*). Theoretical predictions pertaining to the global carbon cycle uses the allometric scaling of metabolic activity (*Allen et al. 2005*).

The physical basis of the scaling exponent would, by induction, also explain the factors and their contributions towards determining metabolic rates. This alluring prospect has resulted in many attempts to explain the scaling relationship. Understanding what determines metabolic rates would have far reaching implications for the origins of life, evolution, cellular biochemistry, and nutrition.

The non-random relationship between metabolic activity and mass, initially described as a correlation, consistently appearing across taxonomic groups cannot be ignored. There is some universal constraint, which has the potential to move us, as a society, one inch closer to the holy grail of understanding life, the universe and everything.

References

1. Allen, A., Gillooly, J. & Brown, J. Linking the global carbon cycle to individual metabolism. *Functional Ecology* **19**, 202–213 (2005).
2. Anfodillo, T. *et al.* An allometry-based approach for understanding forest structure, predicting tree-size distribution and assessing the degree of disturbance. *Proceedings of the Royal Society B: Biological Sciences* **280**, 20122375 (2013).
3. Al-Anzi, B. *et al.* Experimental and computational analysis of a large protein network that controls fat storage reveals the design principles of a signaling network. *PLoS computational biology* **11**, e1004264–e1004264 (May 2015).

4. Bainbridge, B. W. in *Genetics of Microbes* 134–151 (Springer US, Boston, MA, 1987). ISBN: 978-1-4615-7093-6. doi:10.1007/978-1-4615-7093-6_7. <https://doi.org/10.1007/978-1-4615-7093-6_7>.
5. Boitard, L. *et al.* Monitoring single-cell bioenergetics via the coarsening of emulsion droplets. *Proceedings of the National Academy of Sciences* **109**, 7181–7186 (2012).
6. Broach, J. R. Nutritional control of growth and development in yeast. eng. *Genetics* **192**, 73–105. ISSN: 1943-2631 (Electronic); 0016-6731 (Print); 0016-6731 (Linking) (Sept. 2012).
7. Brown, J. H. Towards a Metabolic Theory of Ecology. *Robert H MacArthur Award Lecture* **85**, 228–230. ISSN: 0032-4663 (2004).
8. Burgess, S. C. *et al.* Metabolic scaling in modular animals. *Invertebrate Biology* **136**, 456–472. ISSN: 17447410 (2017).
9. Dungrawala, H. *et al.* Identification of new cell size control genes in *S. cerevisiae*. *Cell division* **7**, 24–24 (Dec. 2012).
10. François, J. & Parrou, J. L. Reserve carbohydrates metabolism in the yeast *Saccharomyces cerevisiae*. *FEMS Microbiology Reviews* **25**, 125–145. ISSN: 0168-6445 (Jan. 2001).
11. Glazier, D. Rediscovering and Reviving Old Observations and Explanations of Metabolic Scaling in Living Systems. *Systems* **6**, 4. ISSN: 2079-8954 (Jan. 2018).
12. Grover, W. H. *et al.* Measuring single-cell density. *Proceedings of the National Academy of Sciences* **108**, 10992–10996 (2011).
13. Hong, S. *et al.* Sub-nanowatt microfluidic single-cell calorimetry. *Nature Communications* **11**, 2982 (2020).
14. Lighton, J. R. B. Limitations and requirements for measuring metabolic rates: a mini review. *European Journal of Clinical Nutrition* **71**, 301–305 (2017).
15. Lu, H. *et al.* A consensus *S. cerevisiae* metabolic model Yeast8 and its ecosystem for comprehensively probing cellular metabolism. *Nature Communications* **10**, 3586 (2019).
16. Makarieva, A. M. *et al.* Mean mass-specific metabolic rates are strikingly similar across life's major domains: Evidence for life's metabolic optimum. *Proceedings of the National Academy of Sciences of the United States of America* **105**, 16994–16999. ISSN: 00278424 (2008).
17. Ratcliff, W. C., Denison, R. F., Borrello, M. & Travisano, M. Experimental evolution of multicellularity. *Proceedings of the National Academy of Sciences of the United States of America* **109**, 1595–1600. ISSN: 00278424 (Jan. 2012).
18. Thommen, A. *et al.* Body size-dependent energy storage causes Kleiber's law scaling of the metabolic rate in planarians. *eLife* **8**, 1–69. ISSN: 2050084X (2019).
19. Yoshioka, K. *et al.* A novel fluorescent derivative of glucose applicable to the assessment of glucose uptake activity of *Escherichia coli*. *Biochimica et Biophysica Acta (BBA) - General Subjects* **1289**, 5–9. ISSN: 0304-4165 (1996).
20. Zaoli, S., Giometto, A., Giezendanner, J., Maritan, A. & Rinaldo, A. On the probabilistic nature of the species-area relation. *Journal of Theoretical Biology* **462**, 391–407. ISSN: 0022-5193 (2019).
21. Zaoli, S., Giometto, A., Marañón, E., *et al.* Generalized size scaling of metabolic rates based on single-cell measurements with freshwater phytoplankton. *Proceedings of the National Academy of Sciences* **116**, 17323–17329. ISSN: 0027-8424 (2019).

Appendix: The Droplet in Droplet Method

To obtain the Droplet in Droplet set-up described in Chapter 3, appropriate microfluidic devices were required, along with suitable continuous phase formulations. This Appendix describes the devices used and their fabrication.

Droplets can simply be obtained by vortexing a mixture of the continuous phase and the disperse phase. The dispersed phase is what goes inside the droplet. The continuous phase is the medium in which droplets are generated. The vortexing method gives no control over the size of the droplet, and the resulting droplets will be polydisperse, i.e. have a wide distribution of droplet sizes. Most microfluidic applications require monodisperse droplets, with minimal variance in droplet sizes. Specialised microfluidic devices are used for controlled formation of monodisperse droplets. A commonly used device configuration for making droplets is a T junction, where the dispersed phase meets the continuous phase perpendicularly. As the dispersed phase flows into the main channel, the shear forces generated by the flow of the continuous phase breaks the stream of the dispersed phase into droplets. A flow focusing device uses symmetric shearing of the dispersed phase by the continuous phase, to facilitate controlled and stable generation of droplets. This type of device can be used for high throughput of droplets (*Teh et al. 2008*).

A flow focusing device and a T junction device have been used in succession to generate the droplet in droplet system.

Microfluidic Devices Used - Flow Focusing

The first objective for making the droplet in droplet system is to obtain the aqueous droplets in oil. A hydrophobic flow focusing device described in Figure 1 is used for this purpose. The phobicity of the channels to the dispersed phase allows for better control over droplet shearing. As described in Figure 1, the continuous phase (oil, yellow) symmetrically shears the dispersed phase (aqueous, blue) to generate mono-disperse droplets. The droplets are collected in a tube containing the oil-surfactant continuous phase. Given the choice of the oil, the aqueous droplets are lighter than the oil and float. The continuous phase here is the fluorinated oil HFE 7500, with 2.5% Pico-SURF surfactant.

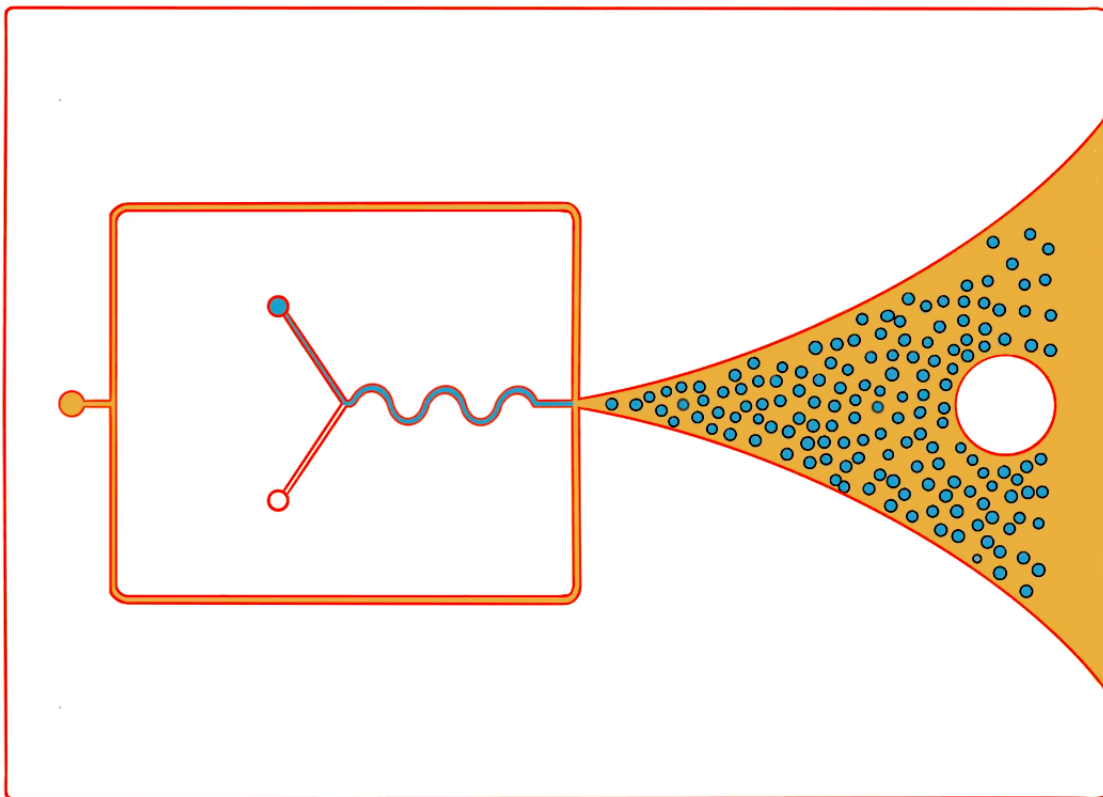


Figure 4.1: A flow focusing device is used for generating mono-disperse aqueous droplets. Image by Akshaya Iyer

The number density of aqueous droplets when pumped into a simple T junction device is very high for having a single aqueous droplet in a large oil droplet. To facilitate the dilution, a device as described in Figure 2 was used. At the Y intersection, the flow rate of the dense-droplet arm is lower than that of the oil-arm. The relative flow rates controls the number density of droplets that reach the T junction. At the T junction, owing to the device configuration and flow rates, large oil droplets are sheared out. The aqueous droplets that flowed into the main channel before the stream is broken by the continuous phase get trapped in the oil droplet. Another important thing to note is that this device needs to be hydrophilic to generate droplets. The continuous phase is aqueous. If the device is not hydrophobic, the oil and water would simply form two parallel streams in the main channel. To make the device hydrophilic the protocol described in Trantidou et al has been used. The device channels are coated with poly-vinyl alcohol (PVA), a hydrophilic polymer. A PVA solution is left inside the channel for 10 minutes. The PVA is then thoroughly removed, and the device is kept at 110 °C for 10 minutes. This process is repeated three times to ensure that the PVA coating is long-lasting (*Trantidou et al. 2017*).

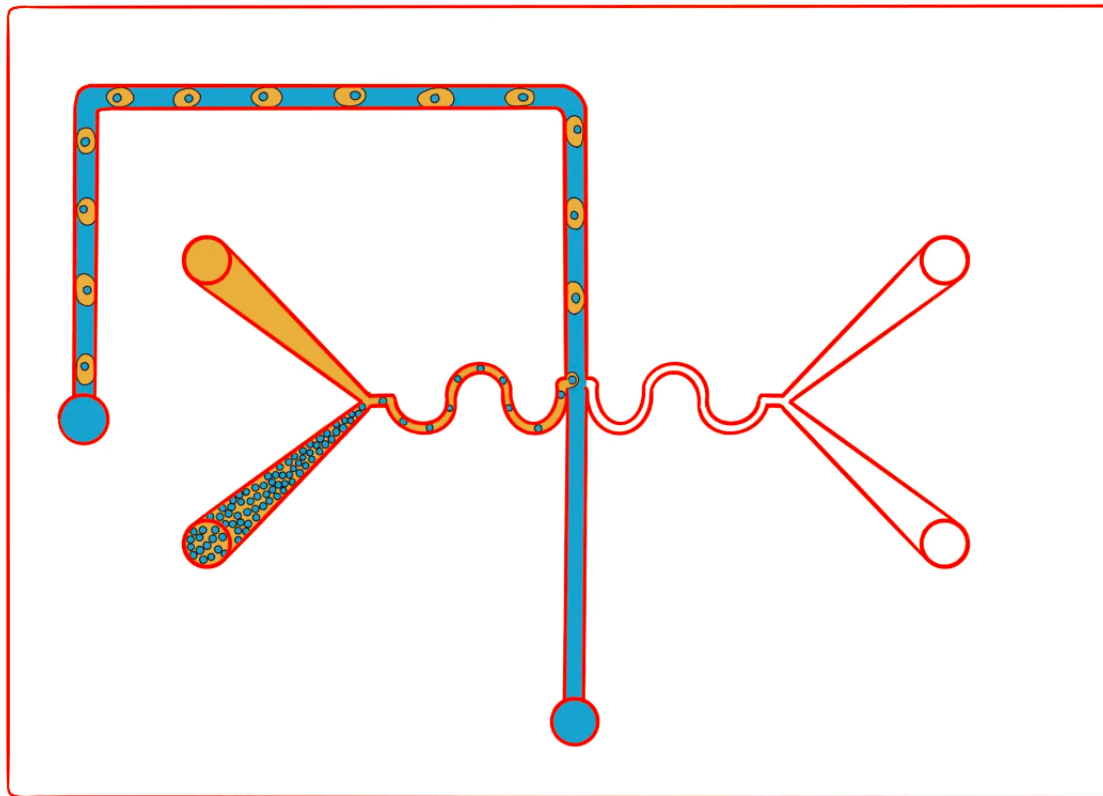


Figure 4.2: T junction device for generating the droplet in droplet setup. Image by Akshaya Iyer

The droplets obtained were pipetted into a chamber on an 8 well chamber slide (Ibidi), and imaged under a microscope. The chamber slide has 8 well separated chambers, with a height of 1cm, on a slide. It is usually used for immunofluorescence protocols; the design allows for cell cultivation, fixation, staining and imaging on the same device.

Device Fabrication

The microfluidic devices used for this protocol were made from using poly-dimethylsiloxane (PDMS). PDMS is an optically clear silicon-based organic polymer. To make a microfluidic device, PDMS is mixed with a cross linking agent and heat-cured on a device mold. The hardened PDMS device, imprinted with the microchannels defined on the mold is then bonded onto a thoroughly cleaned glass slide. Appropriate inlet and outlet holes are punched on the device before bonding. Plasma treatment is used to bond the PDMS device on to the glass slide (*Raj M & Chakraborty 2020*).

The microfluidic mold is made on a Silicon wafer. A uniform layer of the epoxy resin SU-8 is deposited on the wafer. A photomask of the design to be imprinted is placed over the wafer and exposed to UV light. As a result, only the region on the SU-8 coating exposed to UV is cured. The rest of the SU-8 is etched away to obtain the device mold. This fabrication process is done in a clean room (dust free environment) for obtaining precise device molds.

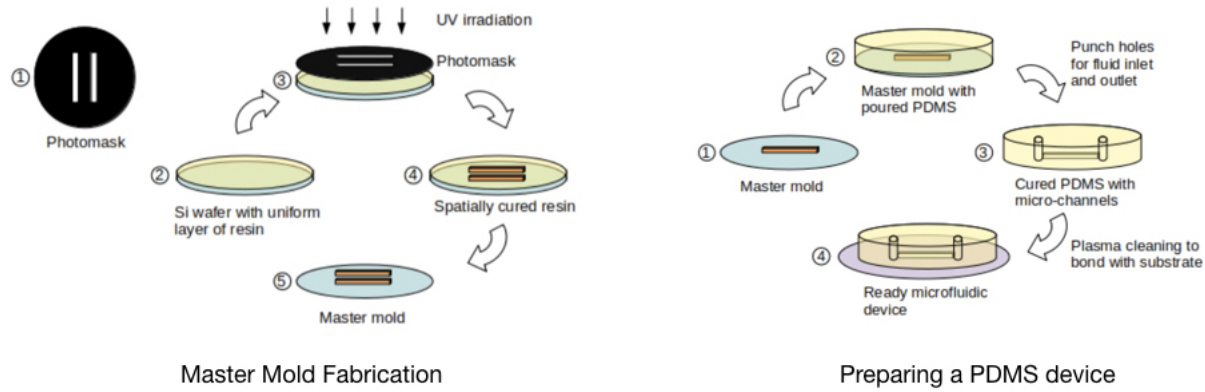


Figure 4.3: Schematic outline for preparing a mold for a device and the PDMS device that can be used for micro-fluidics. Image by Yash Rana

References

1. Raj M, K. & Chakraborty, S. PDMS microfluidics: A mini review. *Journal of Applied Polymer Science* **137**, 48958 (2020).
2. Teh, S.-Y., Lin, R., Hung, L.-H. & Lee, A. P. Droplet microfluidics. *Lab Chip* **8**, 198–220 (2 2008).
3. Trantidou, T., Elani, Y., Parsons, E. & Ces, O. Hydrophilic surface modification of PDMS for droplet microfluidics using a simple, quick, and robust method via PVA deposition. *Microsystems & Nanoengineering* **3**, 16091 (2017).

Acknowledgements

This project was largely made possible with the help of Dr. Shashi Thutupalli, with his constant feedback and support in providing direction. My colleagues, Nishant Narayansamy, Yash Rana and Anton Iyer worked tirelessly alongside me during this project. My lab mates at the Thutupalli Lab at NCBS, Charuhansini Kulkarni, Manoj Kumar, Aniruddh Murali and Anupam Singh have helped immensely, providing useful, actionable feedback and their technical expertise. While affiliated with the project, I had the opportunity to interact with many members of the Simons Center for the Study of Living Machines. Saptarishi Dasgupta, Dr. Amarender Nagilla, Dr. Alex Rautu, and Prof. Madan Rao provided very useful insights for modeling droplet shrinkage in the proposed set-up. I am also thankful for my extremely supportive family. My sister, Akshaya Iyer provided some useful illustrations and graphics for this report.

This project, along with the technical and research experience, allowed me to make connections and conversations that will be forever cherished. I am grateful for the opportunity of being affiliated with both, the National Centre for Biological Sciences, and the Indian Institute of Science. I also thank Kishore Vaigyanik Protsahan Yojana (KVPY) for funding me through my education at the Indian Institute of Science, Bangalore.